JVI Journals.ASM.org

Mouse Prion Protein (PrP) Segment 100 to 104 Regulates Conversion of PrP^C to PrP^{Sc} in Prion-Infected Neuroblastoma Cells

Hideyuki Hara, Yuko Okemoto-Nakamura, Fumiko Shinkai-Ouchi, Kentaro Hanada, Yoshio Yamakawa, and Ken'ichi Hagiwara

Department of Biochemistry and Cell Biology, National Institute of Infectious Diseases, Tokyo, Japan

Prion diseases are characterized by the replicative propagation of disease-associated forms of prion protein (PrP^{Sc}; PrP refers to prion protein). The propagation is believed to proceed via two steps; the initial binding of the normal form of PrP (PrP^C) to PrP^{Sc} and the subsequent conversion of PrP^C to PrP^{Sc}. We have explored the two-step model in prion-infected mouse neuroblastoma (ScN2a) cells by focusing on the mouse PrP (MoPrP) segment 92-GGTHNQWNKPSKPKTN-107, which is within a region previously suggested to be part of the binding interface or shown to differ in its accessibility to anti-PrP antibodies between PrP^C and PrP^{Sc}. Exchanging the MoPrP segment with the corresponding chicken PrP segment (106-GGSYHNQKPWKPPKTN-121) revealed the necessity of MoPrP residues 99 to 104 for the chimeras to achieve the PrP^{Sc} state, while segment 95 to 98 was replaceable with the chicken sequence. An alanine substitution at position 100, 102, 103, or 104 of MoPrP gave rise to nonconvertible mutants that associated with $MoPrP^{Sc}$ and interfered with the conversion of endogenous $MoPrP^C$. The interference was not evoked by a chimera (designated MCM2) in which MoPrP segment 95 to 104 was changed to the chicken sequence, though MCM2 associated with $MoPrP^{Sc}$. Incubation of the cells with a synthetic peptide composed of MoPrP residues 93 to 107 or alanine-substituted cognates did not inhibit the conversion, whereas an anti-P8 antibody recognizing the above sequence in PrP^C reduced the accumulation of PrP^{Sc} after 10 days of incubation of the cells. These results suggest the segment 100 to 104 of $MoPrP^C$ plays a key role in conversion after binding to $MoPrP^{Sc}$.

Transmissible spongiform encephalopathies (TSEs), or prion diseases, are fatal neurodegenerative disorders that include Creutzfeldt-Jakob disease (CJD), variant CJD (vCJD), Gerstmann-Sträussler-Scheinker syndrome (GSS), fatal familial insomnia, and kuru in humans; scrapie in sheep; bovine spongiform encephalopathy (BSE) in cattle; and chronic wasting disease (CWD) in deer. The diseases are characterized by intense neuronal cell loss and vacuolation and an accumulation of the disease-associated form(s) of prion protein (PrP^{Sc}; PrP refers to prion protein) in the central nervous system, though these pathological features do not always correlate with the severity of symptoms (41). While it is still under debate whether the accumulation of PrP^{Sc} in neurons is a direct cause of TSEs (17), the "protein-only hypothesis" (39) claims that the causative infectious agent is PrP^{Sc}, which propagates by conformational conversion of the normal form of cellular prion protein (PrP^C) encoded by the host gene *prnp* (6).

PrP^C is an *N*-glycosylated and glycosylphosphatidylinositol-anchored protein and is sensitive to proteolytic digestion by proteinase K (PK). Nuclear magnetic resonance (NMR)-based analyses of a recombinant mouse PrP (MoPrP) (42) and a recombinant hamster PrP (11) in solution showed that their amino-terminal (N-terminal) halves are flexible, whereas the carboxyl-terminal (C-terminal) domains (residues 121 to 231 for MoPrP) are highly ordered, consisting of three α-helices and two antiparallel β-sheets. A similar structural architecture was determined for recombinant chicken PrP (3). Such structural features likely reflect the structure of PrP^C. In contrast, PrP^{Sc} is partially resistant to PK digestion, with the carboxyl-terminal half left undegraded (32, 40).

The propagation of PrP^{Sc} takes place through a catalytic process requiring the presence of preexisting PrP^{Sc} seeds and recruitment of PrP^C to the preexisting PrP^{Sc}. In prion-infected cells, this process is believed to occur in the lipid rafts of the plasma membrane and/or in the early endocytic pathway (51). Although details of the propagation process are not well understood, lines of evidence have suggested a two-step model in which the initial binding of PrP^C to PrP^{Sc} and the subsequent conformational conversion to PrP^{Sc} are considered distinct events (1, 8, 18, 19). A similar two-step model is argued for the amyloid fibers of the yeast Sup35 protein, known to be the molecular basis for the yeast prion [PSI^+] (46). In MoPrP, the amino acid sequences 95 to 105, 132 to 156, and 220 to 231 have been considered to be in the putative PrP^C-PrP^{Sc} replicative-binding interface, because the accumulation of PrP^{Sc} in mouse neuroblastoma cells infected with scrapie prion (ScN2a cells) (2) was blocked by recombinant Fab fragment antibodies, D13, D18, and R1, raised against these sequences (35, 53). It was also shown that peptides corresponding to the MoPrP residues 88 to 111 and 135 to 157 bound to PrP^{Sc} in an *in vitro* binding assay (29, 30, 48). (The numbering that appeared in references 29, 30, 48, and 53 has been changed to match that of MoPrP in the UniProt database [http://www.uniprot.org, accession number P04925] for ease of comparison. The original numbering in these references has been shifted +1 relative to that in the database.)

From a structural viewpoint, on the other hand, a conformational change was suggested in the region around residues 90 to 120 of hamster PrP (corresponding to 89 to 119 in MoPrP) by the observation that antibodies whose epitopes were mapped to these sequences were able to access PrP^C but not PrP^{Sc} (27, 34, 53). To

Received 19 October 2011 Accepted 24 February 2012
Published ahead of print 7 March 2012
Address correspondence to Ken'ichi Hagiwara, hagiwark@nih.go.jp.

doi:10.1128/JVI.06606-11

date, direct structural elucidation of PrP^{Sc} has not been achieved. However, an analysis by infrared spectroscopy indicated that PrP^{Sc} was abundant in β-sheets (4), and a recent molecular-fitting approach using electron crystallographic density maps suggested an amyloidotic assembly in a trimeric, left-handed parallel, β-helical fold (15, 52). Later, this model was further modified to include two β-helical turns per PrP^{Sc} molecule, based on molecular dynamics (26). Alternatively, molecular dynamics followed by an experimental assessment indicated a spiral model (9, 10). PrP^{Sc} might also fold into a β-sandwich structure (45) like the cross-β spine architecture determined by X-ray crystallography for an amyloid model heptapeptide (GNNQQNY) of the yeast Sup35 protein (31).

In the present study, we focused on residues 92 to 107 of MoPrP (92-GGTHNQWNKPSKPKTN-107) and the corresponding hexadecapeptide of chicken PrP (106-GGSYHNQKPWKPPKTN-121; underlining indicates conserved amino acids), which show modest amino acid sequence homology even though mammalian PrPs and avian PrPs are only distantly related in their whole sequences (36). First, we generated chimeras of MoPrP and chicken PrP to start a framework for the study. Then, the results obtained with mouse-chicken chimeric PrPs were further examined by alanine substitution assays. We show that the MoPrP sequence 100 to 104 (100-KPSKP-104) is critical to the conversion of MoPrP into a PK-resistant form in ScN2a cells and that the segment is an auxiliary binding interface between PrP^C and PrP^{Sc} in the transitional stage of the conversion process.

MATERIALS AND METHODS

Nomenclature, numbering of residues, and plasmid construction. The nomenclature for chimeras used in the present study is based on the terminology of Scott et al. (47), in which, for example, an open reading frame (ORF) of chimeric MoPrP having a Syrian hamster PrP ORF cassette between the KpnI and BglI sites (corresponding to MoPrP amino acid residues 95 to 124) was designated MHM2 (Fig. 1) (47). MHM2 possesses an epitope for the antibody 3F4 (Met-Lys-His-Met, derived from the hamster PrP sequence) and an NdeI site (47). MHM2-Q218K (a gift from K. Kaneko, Tokyo Medical University) is a derivative in which Gln^{218} of MHM2 was replaced by Lys^{218} (21). The numbering of amino acid residues is according to the sequences in the UniProt database (http://www.uniprot.org), accession numbers http://www.uniprot.org/uniprot/P04925 for MoPrP and http://www.uniprot.org/uniprot/P27177 for chicken PrP, respectively. The oligonucleotide primers used in the present study are summarized in Table 1.

For the construction of expression plasmids for MHM2 and MHM2-Q218K, the ORFs of MHM2 and MHM2-Q218K (21) were amplified by PCR using primer set 1, and the PCR products were inserted into a pCI-neo expression vector (Promega, Madison, WI) between the EcoRI and SalI sites. The ORF of chicken PrP was obtained by PCR using primer set 2 and genomic DNA from a broiler chicken as the template. The sequence obtained was identical to that in the GenBank database (http://www.ncbi.nlm.nih.gov/genbank) (accession number M95404.1). After subcloning of the chicken PrP ORF into a pCR2.1 vector (Invitrogen, Carlsbad, CA), an epitope for the antibody 3F4 and an NdeI cleavage site were introduced by PCR mutagenesis using primer set 3, and the ORF of chicken PrP tagged by the 3F4 epitope (designated C4) (Fig. 1) was inserted into the pCI-neo vector using EcoRI and SalI sites. In order to create pCI-MCM2 (Fig. 1 and 2A), in which the 10 amino acid residues 95 to 104 of MHM2 were replaced by the corresponding chicken PrP residues 109 to 118, the ORF of MHM2 was first subcloned into the pIB/V5-His vector (Invitrogen) between the EcoRI and NotI sites, and the vector obtained, pIB/V5-MHM2, was cut by EcoRI and NdeI to delete the N-terminal MoPrP sequence (MoPrP residues 1 to 110). Then, the EcoRI-NdeI gene cassette derived from pCI-C4, encoding the N-terminal part of C4 (residues 1 to 124) (Fig. 1), was ligated to generate a mouse-chicken chimera construct, pIB-C2M2 (Fig. 1). A KpnI cutting site was introduced into the C2M2 sequence by PCR mutagenesis using primer set 4, and a mixture of the KpnI-SalI fragment of pIB-C2M2, the EcoRI-KpnI fragment of MHM2, and the EcoRI-SalI-digested pCI-neo vector was subjected to a ligation reaction all at once to yield pCI-MCM2. For the creation of other chimeras (MCM2/c95-102, MCM2/c95-101, MCM2/c95-100, MCM2/c95-99, MCM2/c95-98, and MCM2/c100-103) or single-amino-acid substitutions (MHM2-N99A, MHM2-K100A, MHM2-P101A, MHM2-S102A, MHM2-K103A, and MHM2-P104A), gene cassettes having mutagenized sequences with an EcoRI site at the 5′ end and an NdeI site at the 3′ end were prepared by PCR by using primer sets 5 to 16 and pCI-MCM2 or pIB/V5-MHM2 as the template. The cassettes were then ligated into EcoRI/NdeI-digested pIB/V5-MHM2, and the resultant cDNAs were transferred into the pCI-neo expression vector using EcoRI and SalI sites. The DNA sequences of all constructs were confirmed using an ABI PRISM 310 genetic analyzer (Applied Biosystems, Foster City, CA).

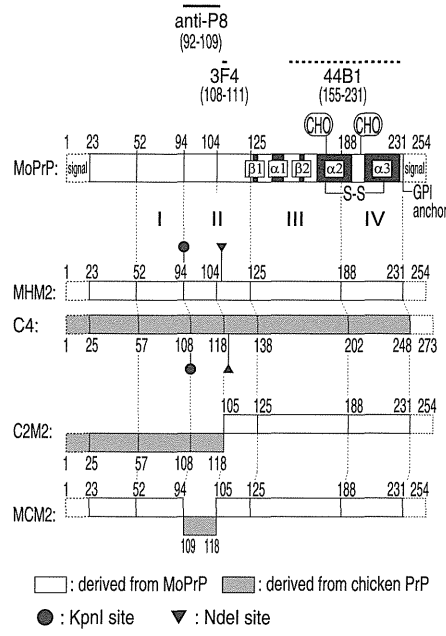

FIG 1 Schematic drawing of chimeric PrP constructs. Protein sequences derived from MoPrP are represented by white bars and those derived from chicken PrP by gray bars. The solid lines with residues in parentheses indicate the locations of continuous epitopes of the anti-P8 and 3F4 antibodies, and the dashed line indicates the location of a discontinuous epitope of the 44B1 antibody. The epitope for antibody 3F4 was introduced into all constructs except MoPrP. The names C4, C2M2, and MCM2 shown on the left refer to the derivation of four domains bordered by restriction enzyme cleavage sites (regions I, II, III, and IV) according to the definition of Scott et al. (47), with M for mouse, H for hamster, and C for chicken PrP, respectively. C4 is equivalent to chicken PrP. The KpnI and NdeI sites were used to generate the chimeras. The boundary amino acid positions shown above the bars are the mouse residue numbers, and those under the bars are the chicken residue numbers. The N-terminal signal sequences for sorting into the endoplasmic reticulum (ER) lumen and the C-terminal signal sequences for addition of the glycosylphosphatidylinositol (GPI) anchor are shown by broken bars. The α-helical and β-sheet structures in recombinant MoPrP (42) are represented by black boxes. The CHO labels denote the potential sites for *N*-glycosylation.

Cell culture and transfection of cells with plasmids. Mouse neuroblastoma N2a cells, and ScN2a cells persistently infected by Chandler/RML scrapie prion (2), were cultured at 37°C in 5% CO_2 in Dulbecco's modified Eagle Medium (Invitrogen) supplemented with 4 mM L-glu-

TABLE 1 Primers used for cloning and mutagenesis of PrP ORFs[a]

No.	ORF	Forward primer (5′–3′)	Reverse primer (5′–3′)
1	MHM2	GgaattcATCATGGCGAACCTTGG	ACGCgtcgacTCATCCCACGATCAGGA
2	Chicken PrP	GgaattcCCGCAGCCATGGCTAGGCTCCTC	ACGCgtcgacGCGAGGACAAGGAACACCCC
3	C4	AAAACCAACATGAAGcatatgGCGGGGGCA	TGCCCCCGCcatatgCTTCATGTTGGTTTT
4	MCM2	CCATCCAGCGGAggtaccTACCACAACCAG	CTGGTTGTGGTAggtaccTCCGCTGGATGG
5	MCM2/c95-102	GgaattcATCATGGCGAACCTTGG	GGCcatatgCTTCATGTTGGTTTTGGGTTTTTTCCATGG
6	MCM2/c95-101	GgaattcATCATGGCGAACCTTGG	GGCcatatgCTTCATGTTGGTTTTGGGTTTGCTCCATGGCTTCTG
7	MCM2/c95-100	GgaattcATCATGGCGAACCTTGG	GGCcatatgCTTCATGTTGGTTTTGGGTTTGCTGGGTGGCTTCTGGTTGTG
8	MCM2/c95-99	GgaattcATCATGGCGAACCTTGG	GGCcatatgCTTCATGTTGGTTTTGGGTTTGCTGGGCTTCTTCTGGTTGTGGTA
9	MCM2/c95-98	GgaattcATCATGGCGAACCTTGG	GGCcatatgCTTCATGTTGGTTTTGGGTTTGCTGGGCTTGTTCTGGTTGTGGTA
10	MCM2/c100-103	GgaattcATCATGGCGAACCTTGG	GGCcatatgCTTCATGTTGGTTTTGGGGGGTTTCCATGGGTTCCACTGATTATG
11	MHM2-N99A	GgaattcATCATGGCGAACCTTGG	GGCcatatgCTTCATGTTGGTTTTTGGTTTGCTGGGCTTAGCCCACTGATTAT
12	MHM2-K100A	GgaattcATCATGGCGAACCTTGG	GGCcatatgCTTCATGTTGGTTTTTGGTTTGCTGGGAGCGTTCCACTG
13	MHM2-P101A	GgaattcATCATGGCGAACCTTGG	GGCcatatgCTTCATGTTGGTTTTTGGTTTGCTAGCCTTGTTCCA
14	MHM2-S102A	GgaattcATCATGGCGAACCTTGG	GGCcatatgCTTCATGTTGGTTTTTGGTTTAGCGGGCTTGTT
15	MHM2-K103A	GgaattcATCATGGCGAACCTTGG	GGCcatatgCTTCATGTTGGTTTTTGGAGCGCTGGGCTT
16	MHM2-P104A	GgaattcATCATGGCGAACCTTGG	GGCcatatgCTTCATGTTGGTTTTAGCTTTGCTGGG

[a] The restriction enzyme sites are shown in lowercase; the mutagenized sequences are underlined.

tamine, 100 U/ml penicillin G, 100 μg/ml streptomycin, and 10% heat-inactivated fetal calf serum (FCS) (Invitrogen) (33). The cells were split at a 10- to 14-fold dilution every 4 to 5 days by dissociation in phosphate-buffered saline (PBS) (SAFC Biosciences, Lenexa, KS) containing 0.05% trypsin and 0.53 mM EDTA (Invitrogen). Plasmids were introduced into the cells (8 μg of DNA per 6-cm dish) using Lipofectamine 2000 reagent (Invitrogen) according to the manufacturer's instructions. At 72 h after transfection, the cells were harvested for Western blot analysis. All proce-

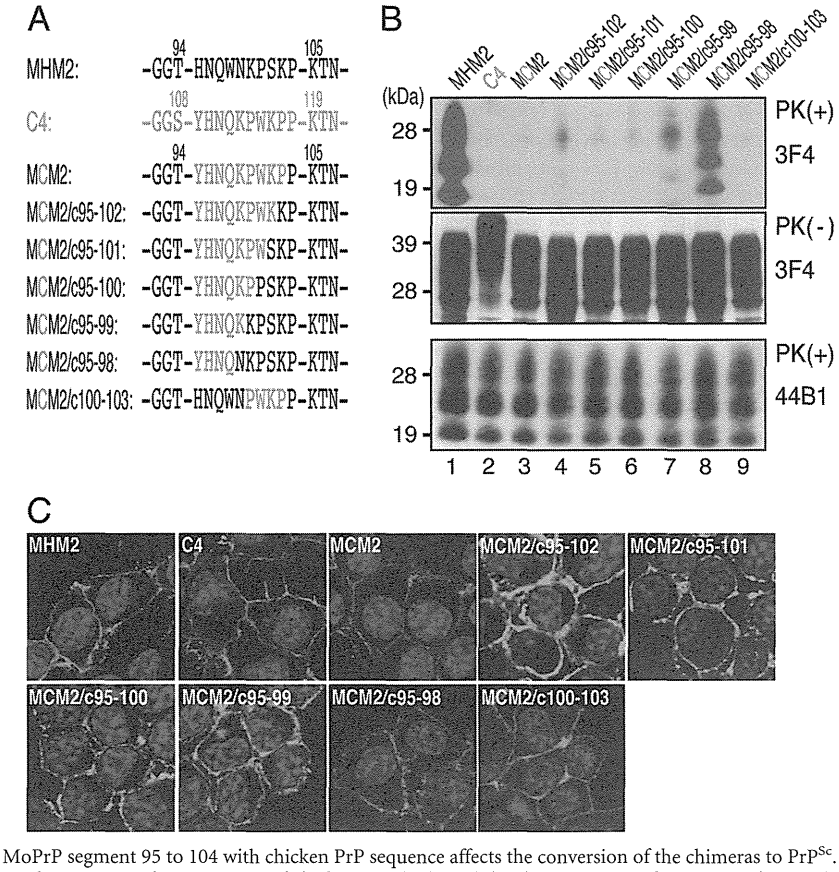

FIG 2 Replacement of the MoPrP segment 95 to 104 with chicken PrP sequence affects the conversion of the chimeras to PrP^{Sc}. (A) Alignment of amino acid residues 92 to 107 of MHM2, the corresponding sequence of chicken PrP (C4), and the chimeric PrPs. The residues derived from C4 are shown in blue. (B) Western blot analysis of cell lysate digested by PK (top and bottom) or lysate without digestion (middle). All the exogenous PrPs possessed the 3F4 epitope. The Western blotting membranes detected by antibody 3F4 show relative amounts of PrP^{Sc} derived from the exogenous PrPs (top) and the relative expression levels of the exogenous PrPs (middle). The antibody 44B1 was used to evaluate the total amount of PrP^{Sc} (i.e., endogenous and exogenous PrP^{Sc}) (bottom). Molecular masses are shown. (C) Immunofluorescence analysis of the localization of the exogenously expressed PrPs (MHM2, C4, or the chimeras) in ScN2a cells. The cells were treated with 1 M guanidine hydrochloride for 3 min and stained for PrP using antibody 3F4 and Alexa Fluor 488-conjugated anti-mouse IgG (green). The nuclei were stained with DAPI (blue).

dures were carried out according to the biosafety guidelines of the National Institute of Infectious Diseases.

Proteinase K treatment of the cell lysate. All procedures were carried out at 4°C. The cells were rinsed three times with 5 ml of PBS (SAFC Biosciences), dissolved with 1 ml of lysis buffer (20 mM Tris-HCl buffer, pH 7.4, containing 0.5% Triton X-100, 0.2% sodium deoxycholate, and 100 mM NaCl) by pipetting, and then centrifuged at 1,500 × *g* for 5 min in an ARO15-24 rotor (Tomy Seiko, Tokyo, Japan) to remove insoluble debris. The concentration of protein in the lysate was determined with a bicinchoninic acid (BCA) protein assay kit (Pierce, Rockford, IL) and bovine serum albumin (Pierce) as a standard, and the lysate was adjusted to 1 mg of protein/ml with the lysis buffer. To prepare samples for the analysis of PrP^{Sc}, aliquots of 800 μl of the lysate were digested with 10 μg of PK (Roche Applied Science, Basel, Switzerland) at 37°C for 1 h. Then, the reaction was terminated with the addition of 20 μl of 20 mM phenylmethylsulfonyl fluoride (Sigma, St. Louis, MO) in methanol. The insoluble materials were collected as precipitates by centrifugation (90,700 × *g*; 1 h) in a TLA-55 rotor (Beckman Coulter, Fullerton, CA), and the precipitates were washed with 500 μl of ice-cold methanol by centrifugation (13,000 × *g*; 30 min) in the ARO15-24 rotor. The pellet was dissolved in 40 μl of a sodium dodecyl sulfate (SDS) sample buffer (62.5 mM Tris-HCl buffer, pH 6.8, containing 5% SDS, 2 M urea, 4% β-mercaptoethanol, 5% glycerol, 0.04% bromophenol blue, and 3 mM EDTA) and heated at 95°C for 10 min. Aliquots of 5 μl of the PK-digested lysate were subjected to SDS-polyacrylamide gel electrophoresis (SDS-PAGE) for Western blot analysis. To examine the total amount of PrP in the cell lysate, aliquots of 5 μl of the non-PK-digested lysate (containing 5 μg of protein) were also subjected to Western blotting.

Western blot analysis. Proteins were resolved by SDS-PAGE using 12% NuPAGE Bis-Tris gels in morpholinopropanesulfonic acid (MOPS)-SDS running buffer (Invitrogen) and transferred to polyvinylidene difluoride membranes (Invitrogen). After blocking treatment with 10 ml of 1% skim milk (Difco-BD Biosciences, Franklin Lakes, NJ) in PBST (PBS containing 0.1% Tween 20) for 1 h, the membranes were washed three times with 50 ml of PBST for 5 min and probed with 10 ml of anti-PrP antibody 3F4 (1:10,000; Millipore, Billerica, MA), anti-PrP antibody 44B1 (1:10,000) (22), or anti-actin antibody (1:10,000; Chemicon-Millipore) overnight at 4°C in PBST containing 0.5% skim milk. The membranes were then washed three times with 50 ml of PBST for 5 min each time and probed with 10 ml of a horseradish peroxidase-labeled anti-mouse IgG (H+L) (1:20,000; KPL, Gaithersburg, MD) for 1 h in PBST containing 0.5% skim milk. After three washes with 50 ml of PBST for 5 min, immunoreactive proteins were detected using ECL Plus Western Blotting Detection Reagents (GE Healthcare, Uppsala, Sweden) with a LAS-1000plus chemiluminescence imaging system (Fuji Film, Tokyo, Japan). Signal intensities were determined by Image Gauge software (Fuji Film) using the integrated peak volume quantification mode.

Binding of PrP^C to PrP^{Sc}. The efficacy with which PrP^C bound to PrP^{Sc} was examined by a previously described method with a slight modification (38). The cells were rinsed with PBS at 72 h after transfection and dissolved in lysis buffer supplemented with a proteinase inhibitor cocktail (Complete Mini; Roche Applied Science, Indianapolis, IN). After the removal of insoluble debris by centrifugation (1,500 × *g*; 5 min) at 4°C in the ARO15-24 rotor, the protein concentration in the lysate was determined with the BCA protein assay kit, and the lysate was adjusted to 1 mg of protein/ml with lysis buffer. Then, aliquots of the lysate (100 μl) were incubated at 37°C overnight and centrifuged at 15,000 × *g* for 10 min at room temperature in the ARO15-24 rotor. The supernatant was transferred to a new tube, and the pellet was suspended in 100 μl of lysis buffer. The supernatant and pellet were then added to 10 volumes of ice-cold methanol, and proteins were precipitated by centrifugation at 13,000 × *g* for 30 min at 4°C in the ARO15-24 rotor. The precipitated proteins were dissolved in 20 μl of SDS sample buffer, heated for 10 min at 95°C, and subjected to Western blot analysis.

Immunofluorescence analysis. The cells were cultured in 35-mm glass bottom dishes (12 mm in diameter; Asahi Glass Co., Ltd., Chiba. Japan) to 50% confluence at 37°C. All manipulations were done at room temperature unless otherwise stated. The cells were washed three times with 2 ml of PBS and fixed with 150 μl of Cytofix fixation buffer (BD Biosciences, Franklin Lakes, NJ) for 15 min. The cells were then washed three times with 2 ml of PBS, permeabilized by incubation with 150 μl of 0.1% Triton X-100 in PBS for 10 min, washed three times with 2 ml of PBS, and treated with 150 μl of 1 M guanidine hydrochloride for 0 to 10 min to retrieve the immunoreactivity of PrP^{Sc} (50). After three washes with 2 ml of PBS, the cells were incubated with 150 μl of 10% FCS in PBS for 30 min for blocking and then with either of the following antibodies in 150 μl of PBS: the anti-PrP antibody 3F4 (Millipore) at 1:1,000 for 1 h at room temperature or anti-P8 (44) at 1:200 overnight at 4°C. After removal of the excess antibodies by washing with 2 ml of PBS three times, the cells were incubated with the following secondary antibodies and 4′,6-diamidino-2-phenylindole (DAPI) (1 μg/ml; Dojindo Laboratories, Kumamoto, Japan) in 150 μl of PBS for 1 h; an Alexa Fluor 488-conjugated goat anti-mouse IgG antibody (Invitrogen) at 1:2,000 for the antibody 3F4 or an Alexa Fluor 488-conjugated goat anti-rabbit IgG antibody (Invitrogen) at 1:2,000 for the anti-P8 antibody. The cells were mounted in Fluoromount-G (SouthernBiotech, Birmingham, AL) and observed using an FV-1000 confocal microscope (Olympus, Tokyo, Japan) with Fluoviewer software (Olympus).

Treatment of the cells with anti-PrP antibody or peptides. To the culture medium of ScN2a and N2a cells in 6-well plates, anti-P8 antibody (raised in a rabbit in our laboratory; the epitope is included in residues 92 to 109 of MoPrP) (44) was added at a final concentration of 0 to 10 μg/ml. The cells were cultured for 10 days with two passages on days 3 and 6 before harvest. As a control, the cells were treated with rabbit normal IgG (R&D Systems, Inc., Minneapolis, MN) in the same way. Peptides derived from the amino acid sequence (positions 93 to 107) of MoPrP were synthesized by 9-fluorenylmethyloxycarbonyl solid-phase chemistry (Operon Biotechnologies, Tokyo, Japan). Their amino acid sequences were GTHNQWNKPSKPKTN (PrP_93-107), GTHNQWNAPSKPKTN (PrP_K100A), GTHNQWNKPAKPKTN (PrP_S102A), GTHNQWNKPSAPKTN (PrP_K103A), and GTHNQWNKPSKAKTN (PrP_P104A). The purity of the peptides was verified by reversed-phase high-performance liquid chromatography (RP-HPLC) and matrix-assisted laser desorption time-of-flight mass spectrometry (purity, >90%). The peptides were dissolved in distilled water at a concentration of 5 mM and added to the culture medium of ScN2a cells in 6-well plates at a final concentration of 10 or 100 μM (33). The cells were cultured for 10 days with two passages on days 3 and 6 before harvest. The stability of the peptides during the cell treatment was examined as follows by using PrP_93-107 as a representative peptide. ScN2a cells were seeded in 24-well plates containing 500 μl of the culture medium per well, and the peptide was added to the medium on day 0 at a final concentration of 100 μM. After cultivation of the cells in triplicate for 0, 1, 2, 3, and 4 days at 37°C, the medium and the cells were retrieved by pipetting up and down. Aliquots of 470 μl of the cell suspension in the medium were added with 30 μl of 100% (wt/vol) trichloroacetic acid (TCA) (Nacalai Tesque, Inc., Kyoto, Japan); then, the samples were centrifuged at 12,000 × *g* for 10 min at 4°C for deproteinization, and the supernatant was stored at −80°C until analysis. The peptide was also incubated in the medium, but without the cells, and was processed in the same way. For quantification of the peptide, aliquots of the supernatant were diluted 10 times with distilled water, and 20 μl of the diluted supernatant (equivalent to 188 pmol of the peptide if no degradation had occurred) was subjected to RP-HPLC on an LC-2000Plus system (Jasco, Tokyo, Japan) equipped with a fluorescence detector (FP-2020Plus; Jasco) and an Inertsil ODS-2 column (4.6 mm by 150 mm; GL Sciences, Tokyo, Japan). Elution was carried out at 40°C by a linear gradient from 100% solution A (5% acetonitrile-water, 0.05% trifluoroacetic acid [TFA]) to 10% solution B (60% acetonitrile-water, 0.05% TFA) in 32 min at a flow rate of 0.8 ml/min. PrP_93-107 was detected by fluorescence

(excitation at 280 nm/emission at 320 nm) derived from a tryptophan residue in its amino acid sequence. PrP_93-107 was eluted at approximately 22 min. The amounts of PrP_93-107 were determined by peak height in the chromatogram in comparison with the peak height of 188 pmol of PrP_93-107 as a standard.

RESULTS

Mutagenic analysis with chicken PrP gene cassettes identified MoPrP residues 99 to 104 as a critical segment. To explore the roles of region 95 to 104 of MoPrP in prion propagation, we took advantage of the limited homology in the region between MoPrP and chicken PrP and used gene cassette-based mutagenesis to generate a series of mouse-chicken chimeric PrPs (Fig. 1 and 2A). In order to distinguish the exogenously expressed PrPs from the endogenous MoPrP in N2a and ScN2a cells (2), the exogenous PrPs were tagged with the epitope for the antibody 3F4 (Met-Lys-His-Met) (28, 47). MHM2 (MoPrP possessing the 3F4 epitope) was converted efficiently to PrP^{Sc} in ScN2a cells (Fig. 2B, top, lane 1), consistent with a previous report (47). Under these conditions, the expression of C4 (i.e., 3F4 epitope-tagged chicken PrP) and all seven chimeras (Fig. 2A) was comparable to that of MHM2 (Fig. 2B, middle). As expected given the species barrier to prion infection (41), C4 could not be converted to a PK-resistant form (Fig. 2B, top, lane 2). Among the chimeras with chicken sequences of various lengths, MCM2/c95-98, in which the MoPrP residues 95 to 98 (HNQW) were replaced by the chicken sequence YHNQ but residues 99 to 104 were unchanged, was converted to a PK-resistant form almost as efficiently as MHM2 (Fig. 2B, top, lane 8). Conversely, MCM2/c100-103, in which MoPrP residues 100 to 103 were replaced with the chicken sequence, failed to be converted (Fig. 2B, top, lane 9). The other five chimeras, in which the chicken cassettes extended further to the C-terminal side (up to residues 99, 100, 101, 102, and 103), were also incapable of changing into PK-resistant forms (Fig. 2B, top, lanes 3 to 7). The nonconvertibility of the chimeras was unlikely to have been due to mislocalization of the chimeric PrPs in the cells, since immunofluorescence analysis showed similar distributions of these chimeras and MHM2 on the plasma membrane and in intracellular punctate compartments (Fig. 2C). Accordingly, we concluded that residues 99 to 104 of MoPrP (99-NKPSKP-104) include key residues for inducing the conversion of PrP^{C} to the PrP^{Sc} state.

Alanine scanning refined the key residues in MoPrP 99 to 104. Based on the results obtained with the mouse-chicken chimeras, we next narrowed down the area crucial for the conversion of PrP^{C} to PrP^{Sc} by replacing single amino acids in the MoPrP 99-to-104 segment with alanine (Fig. 3A). As shown in Fig. 3, Western blot analysis (Fig. 3B, middle; probed by the antibody 3F4) and immunofluorescence analysis (Fig. 3C) indicated the expression levels and cellular localization of the 3F4 epitope-tagged alanine-substituted mutants were comparable to those observed for MHM2. Under these conditions, the replacement of Pro^{101} with Ala (designated the P101A mutant), a mutation analogous to P102L identified in patients with the inherited prion disease GSS (20), gave rise to PK-resistant PrP^{Sc} as efficiently as MHM2 (Fig. 3B, top, lane 5). Also, N99A was a moderately convertible mutant. In contrast, the K100A mutant was almost nonconvertible, though a small amount of PrP^{Sc} was still detectable by Western blot analysis (Fig. 3B, top, lane 4). The replacement of Ser^{102}, Lys^{103}, or Pro^{104} (S102A, K103A, and P104A, respectively) completely prevented conversion into PrP^{Sc} in the cells (Fig. 3B, top, lanes 6 to 8). Although P104A of MoPrP was analogous to the human PrP Pro^{105}-to-Leu mutation identified in patients with another type of GSS (24, 25, 54), it was nonconvertible in the present experimental setting. The conversion efficacy of this type of mutation might be synergistic with additional factors, for example, the co-occurrence of polymorphic variation at codon 129 (methionine or valine) (25, 54). The K100A, S102A, K103A, and P104A mutants not only were nonconvertible themselves, but also blocked conversion of the endogenous PrP^{C} to PrP^{Sc} (Fig. 3B, top and bottom, lanes 4 and 6 to 8) at levels similar to those of MHM2-Q218K, which was known as a "dominant-negative" mutant (21, 23) (Fig. 3B, top and bottom, lane 9). Taken together, the amino acid residues Lys^{100}, Ser^{102}, Lys^{103}, and Pro^{104} of MoPrP were critical for inducing the conversion of PrP^{C} to the PrP^{Sc} state.

Residues 100 to 104 play a pivotal role in the conversion. Next, we examined whether changes in the amino acid sequence 100 to 104 of MoPrP affects the binding of PrP^{C} to PrP^{Sc} or the subsequent conversion step (1, 8, 18, 19). To distinguish the two steps, we performed a biochemical assay to detect the formation of a complex of PrP^{C} with PrP^{Sc}. This assay is based on the notion that the newly synthesized PrP^{C} bound to preexisting PrP^{Sc} is converted to PrP^{Sc} and finally assimilated into the PrP^{Sc} aggregates, so that all such temporary complexes and resultant aggregates may be recovered in the pellet after centrifugation of the cell lysate.

In N2a cells, approximately 70 to 82% of the exogenously expressed PrPs were recovered in the supernatant (Fig. 4A and B), while 20 to 30% of them were recovered in the pellet at background levels in the absence of PrP^{Sc}. When the lysate of ScN2a cells expressing MHM2 (the convertible control) was fractionated by centrifugation, as much as 75% of exogenously expressed MHM2 was retrieved in the pellet (Fig. 4C and D, lanes 1). MCM2 (Fig. 4C, lane 2, and D, lane 4) and the alanine-substituted mutants (Fig. 4C, lanes 3 to 8) were retrieved in the pellet in a manner similar to that of MHM2. Interestingly, 60% of C4 was recovered in the supernatant in ScN2a cells, whereas C2M2 and MCM2 (a nonconvertible chimera, as shown in Fig. 2B, lane 3) were retrieved in the pellet at levels comparable to that of MHM2 (the convertible control) (Fig. 4D). The difference between C2M2 and C4 was in their C-terminal halves: C2M2 had the chicken PrP sequence residues 1 to 118 followed by the MoPrP sequence residues 105 to 231 (Fig. 1). This difference was also present for MCM2 and C4 (Fig. 1). Accordingly, the data shown in Fig. 4D suggest a predominant binding interface for PrP^{Sc} in the C-terminal half of PrP^{C} (residues 105 to 231 in the MoPrP sequence). It also should be noted that as much as 40% of C4 expressed in ScN2a cells was fractionated into the pellet (Fig. 4D), approximately 20% of which was ascribed to the background level independent of PrP^{Sc} (Fig. 4B) while the remaining 20% was due to the association of C4 and $MoPrP^{Sc}$. The question remains whether such association of C4 with $MoPrP^{Sc}$ occurs by interaction of particular segments of chicken PrP (C4) with $MoPrP^{Sc}$. The results obtained by these chimeras, together with the nonconvertibility of the alanine-substituted mutants in binding to PrP^{Sc} (Fig. 3 and 4), suggested that segment 100 to 104 was involved in the conversion and, consequently, in the growth of PrP^{Sc} aggregates.

Residues 92 to 109 of MoPrP are cryptic in the PrP^{Sc} form. A previous study using a panel of antibodies in a cell-free enzyme-linked immunosorbent assay suggested a structural change in residues 90 to 120 of hamster PrP between PrP^{C} and PrP^{Sc} (34). This

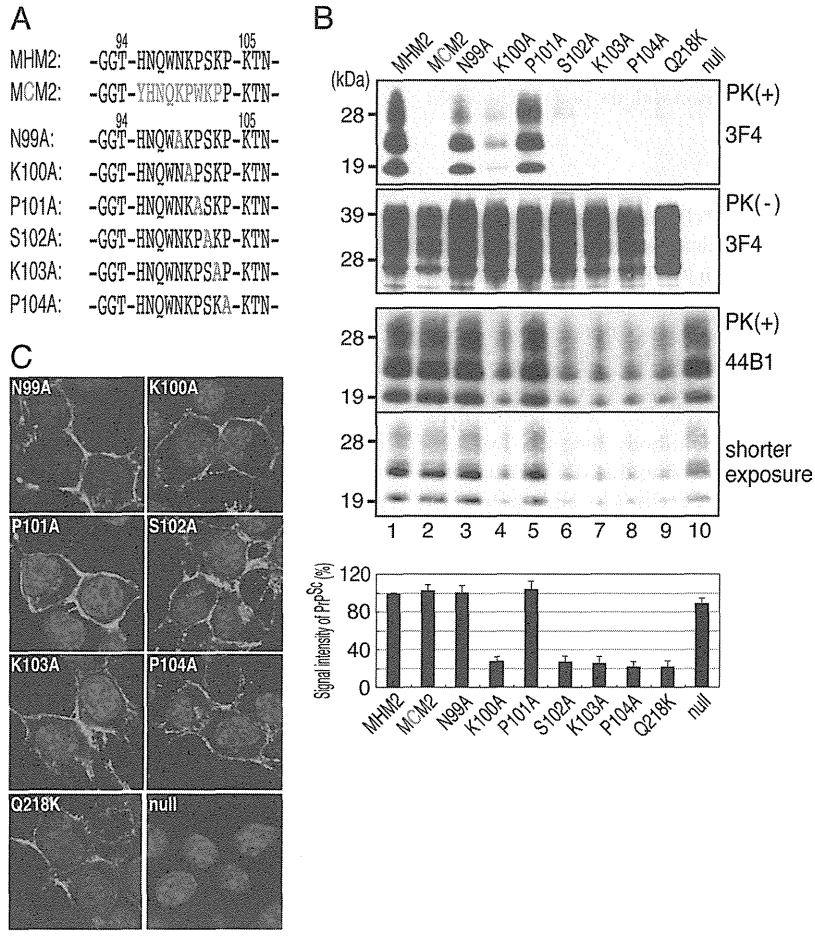

FIG 3 Replacement of the amino acid residue at position 100, 102, 103, or 104 of MoPrP with alanine inhibits the conversion of the mutants and endogenous PrP^C to PrP^{Sc}. (A) Alignment of residues 92 to 107 of MHM2, MCM2, and the alanine-substituted mutants. The residues derived from C4 are shown in blue. The substituted alanine is shown in red. (B) Western blot analysis of cell lysate digested by PK (top and bottom) or lysate without digestion (middle). All the exogenous PrPs possessed the 3F4 epitope. The membranes represent the amounts of PrP^{Sc} converted from the exogenous PrPs (top; detected by antibody 3F4), the expression levels of the exogenous PrP (middle; antibody 3F4), and the total amount of PrP^{Sc} (i.e., endogenous and exogenous PrP^{Sc}) (bottom two images; antibody 44B1) in ScN2a cells. The two bottom images of the same membrane with different exposure times show that the signals detected by antibody 44B1 are not saturated but are within the range of the chemiluminescence imaging system. The signal intensities of PrP^{Sc} bands detected by antibody 44B1 were quantified and expressed as percentages of that of MHM2, with 0% denoting an undetectable level of PrP^{Sc} (invisible band). The data represent the means and standard errors of the mean (SEM) for three independent experiments. (C) Immunofluorescence analysis of the localization of the alanine-substituted PrPs and Q218K in ScN2a cells. Null denotes untransfected ScN2a cells. The cells were treated with 1 M guanidine hydrochloride for 3 min and stained for PrP using antibody 3F4 and Alexa Fluor 488-conjugated anti-mouse IgG (green). The nuclei were stained with DAPI (blue).

was based on the observation that the antibodies, for example, D4, D13, and R10, whose epitopes were mapped in this region (35), were reactive to PrP^C but not to PrP^{Sc} unless it was denatured by guanidine thiocyanate (34, 53). Following this observation, we examined if an antibody raised against residues 92 to 109 of MoPrP (designated the anti-P8 antibody) (44) would bind to PrP^C but not to PrP^{Sc} in N2a and ScN2a cells. In an immunofluorescence analysis, the anti-P8 antibody gave an unchanged level of immunopositive signals for PrP^C in N2a cells irrespective of pretreatment of the cells with 1 M guanidine hydrochloride (Fig. 5, top row). Such a staining pattern for N2a cells is similar to that previously reported for PrP^C in N2a cells using the antibody 6H4 (51). In ScN2a cells, the anti-P8 antibody gave much weaker signals for cells without the guanidine treatment (Fig. 5, compare the left column). However, it gave rise to an increased intensity of staining after guanidine treatment for 5 min (Fig. 5, bottom row), though it was uncertain whether the effect of 1 M guanidine was in unfolding PrP^{Sc} aggregates or in dispersion of an unidentified molecule(s) associated with PrP^{Sc} to unmask the epitope. These results suggest that the epitope for anti-P8 antibody is accessible in PrP^C, and the epitope might be hindered in access in the PrP^{Sc} state unless the cells are treated with guanidine (see Discussion).

Anti-P8 antibody inhibited the propagation of PrP^{Sc} in ScN2a cells, but synthetic peptides derived from MoPrP residues 93 to 107 did not. As described above, the anti-P8 antibody is expected to bind to PrP^C but not to PrP^{Sc} in ScN2a cells. Thus, to further support the involvement of Lys^{100}, Ser^{102}, Lys^{103}, and Pro^{104} in the conversion step, we cultivated ScN2a cells in the presence of the anti-P8 antibody for 10 days, during which time the antibody should bind to PrP^C in the cells. The amount of PrP^{Sc}

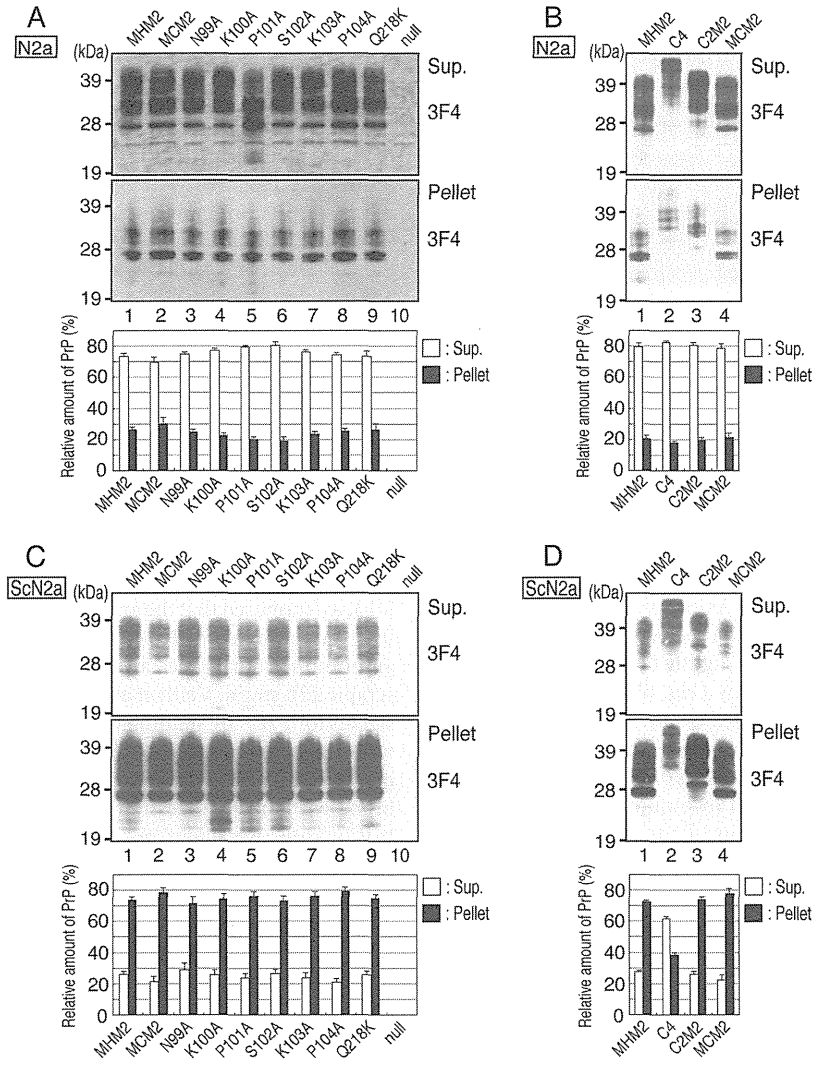

FIG 4 Replacement of MoPrP segment 99 to 104 by the chicken sequence does not affect binding of the chimeric PrP to PrP^{Sc}. (A and B) N2a cells transfected with the expression vectors encoding MHM2, MCM2, the alanine-substituted mutants, or Q218K (A) and C4 or C2M2 (B) were subjected to a fractionation assay, followed by Western blot analysis. PrPs recovered in the supernatant (Sup.) (A and B, top) and the pellet (A and B, middle) were detected by antibody 3F4. MHM2 (A and B, lanes 1) and Q218K (A, lane 9) were examined as references, while null (A, lane 10) represents untransfected N2a cells. The signal intensities of the PrP bands detected in the supernatant and pellet were quantified and expressed as percentages of the total amount of 3F4-positive PrP in the cells (A and B, bottom). The data represent the means ± SEM for four independent experiments. (C and D) The same experiment as in panels A and B was carried out using ScN2a cells. Exogenous PrPs associated with PrP^{Sc} aggregates were recovered in the pellet (C and D, middle), while those free from PrP^{Sc} aggregates were found in the supernatant (C and D, top). The signal intensities of the PrP bands detected in the supernatant and pellet were quantified and expressed as percentages of the total amount of 3F4-positive PrP in the cells (C and D, bottom). The data represent the means ± SEM for four independent experiments.

decreased depending on the dosage of the antibody (Fig. 6A, top, lanes 1 to 4), whereas rabbit normal IgG (the control) was ineffective (Fig. 6A, top, lanes 5 to 8). Western blot analysis of the samples not digested by PK (Fig. 6A, middle) detected 25- to 40-kDa bands that corresponded to the full-length forms of the di-, mono-, and nonglycosylated PrP (f-PrP), including PrP^{Sc} and newly synthesized PrP^{C}, and 19- to 25-kDa bands that were attributed to remnant PrP^{Sc} (r-PrP) partially resistant to cellular endogenous proteases (33). Since the anti-P8 antibody did not affect the amount of f-PrP (Fig. 6A, middle, lane 4) but predominantly eliminated r-PrP, it was considered not to interfere with the *de novo* synthesis of PrP^{C}, and thus, the clearance of PrP^{Sc} in the cells was not due to a reduction in the supply of PrP^{C} to be converted. The inhibitory effect of the anti-P8 antibody on the conversion of PrP^{C} to PrP^{Sc} might be ascribed either to the masking of a putative primary binding site or to clamping of the epitope of PrP^{C} to hamper the structural change. To examine this point, we incubated ScN2a cells with a synthetic peptide composed of residues 93 to 107 of the wild-type MoPrP, which corresponded to the core sequence of the anti-P8 antibody's epitope, or a cognate peptide in which either Lys^{100}, Ser^{102}, Lys^{103}, or Pro^{104} was replaced with Ala (Fig. 6C). The peptides were added to the culture medium, and the cells were cultured for 10 days, with two passages on days 3 and 6 in fresh medium containing peptides before harvest. The peptides, however, did not reduce the accumulation of PrP^{Sc} in the cells (Fig. 6B). We asked if the ineffectiveness of the peptides was as-

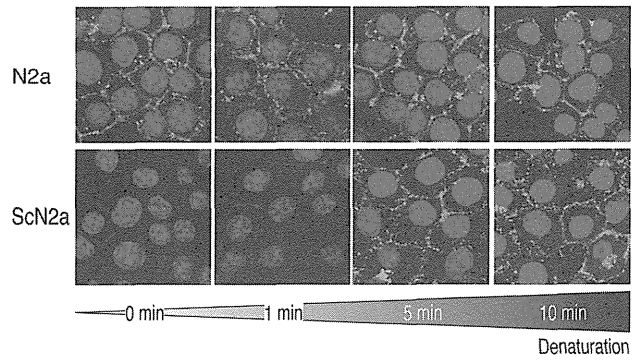

FIG 5 Anti-P8 antibody can bind to PrP^C but not PrP^{Sc} in ScN2a cells under native conditions. N2a cells or ScN2a cells were pretreated with 1 M guanidine hydrochloride for 0 to 10 min as specified below and then incubated with the anti-P8 antibody and Alexa Fluor 488-conjugated secondary antibodies for detection of endogenous MoPrPs (green). The nuclei were stained with DAPI (blue). The images of confocal microscopy were collected by setting the detector gain at the same level.

cribed to their rapid degradation. As examined with a representative peptide, PrP_93-107, the loss of the peptide at the initial concentration of 100 μM proceeded slightly faster in the presence of the cells than in the medium only (Fig. 6D). We observed that about 60% of PrP_93-107 remained on day 3, and its half-life was 4 days in the cell culture (Fig. 6D, solid line). This excluded the possibility of rapid degradation and loss of the peptides during the treatment of the cells. Analysis of recombinant MoPrP by NMR spectroscopy suggested the region of the amino acid sequence from residues 93 to 107 of $MoPrP^C$ is not constrained in solution (42), and we expect the synthetic peptides corresponding to this region are structurally as flexible as the region in the PrP^C molecule. Accordingly, if this region of the PrP^C molecule interacts with and is accommodated in particular sites of PrP^{Sc}, we suppose that the synthetic peptides similarly could mimic the corresponding region of the PrP^C molecule. The lack of competitive inhibition of the propagation of PrP^{Sc} by the peptides suggested that the predominant binding interface of PrP^C-PrP^{Sc} was outside residues 93 to 107 of MoPrP, conceivably in the C-terminal domain of MoPrP, as described above (Fig. 4). Although residues 93 to 107 are not involved in the primary binding interface, we see a possibility that they participate in an auxiliary binding interface. The effect of the anti-P8 antibody might be ascribed to either clamping of the epitope of PrP^C or masking of any putative auxiliary binding interfaces near the epitope, preventing the conversion of PrP^C to PrP^{Sc} from proceeding.

DISCUSSION

Replicative propagation of disease-associated forms of prion protein (PrP^{Sc}) through conversion of the normal form of prion protein, PrP^C, is a hallmark of transmissible spongiform encephalopathies. This process is considered to occur in two kinetically distinguishable steps (1, 8, 18, 19): the initial binding of PrP^C to preexisting PrP^{Sc} and the subsequent conversion of PrP^C into PrP^{Sc}. In the present study, we focused on residues 92 to 107, part of the conformationally heterogeneous and flexible region of a recombinant MoPrP (42) but found at the distal N-terminal end of PrP^{Sc} after PK digestion (32, 40).

A previous report speculated that residues 90 to 104 and 106 to 115 in hamster PrP (corresponding to 89 to 103 and 105 to 114 in MoPrP, respectively) might not participate in the initial binding because two antibodies (one against 90 to 104 and the other, antibody 3F4, against 106 to 115) did not inhibit the generation of a PK-resistant form(s) of PrP in an *in vitro* cell-free conversion system (18). The results of the present study, indicating that MoPrP residues 100 to 104 (KPSKP) play a role in the conversion rather than as a predominant binding interface during prion propagation, seem to support the above notion. However, in contrast to the cell-free conversion assay, which showed that the antibody against hamster PrP residues 90 to 104 did not block the formation of a PK-resistant form(s) of PrP (18), the incubation of ScN2a cells with the anti-P8 antibody whose epitope was in MoPrP residues 92 to 109 decreased the amount of PrP^{Sc} in the present study (Fig. 6A, top, lanes 1 to 4). In this regard, Peretz et al. (35) reported that the incubation of ScN2a cells with the Fab fragment antibody D13 (10 μg/ml), which was specific to MoPrP residues 95 to 105 (27, 35, 53), disrupted the propagation of PrP^{Sc}. They ascribed this inhibition to the D13 antibody's binding to the PrP^C molecule on the cell surface, thereby masking a putative PrP^C-PrP^{Sc} binding interface in the proximity of the epitope (35). Like the antibody D13, we supposed that the anti-P8 antibody preferentially binds to PrP^C rather than to PrP^{Sc} on the cell surface (Fig. 5). However, in an immunofluorescence analysis of ScN2a cells infected with the scrapie 22L strain, Veith et al. (51) reported that immunopositive signals for PrP^{Sc} by staining with antibody 6H4 after PK digestion were noticeable in intracellular areas than at the plasma membrane and that the immunopositive signals at the plasma membrane without PK digestion could be caused by both PrP^C and PrP^{Sc}. Thus, we might not be clearly discriminating PrP^C and PrP^{Sc} at the plasma membrane shown in Fig. 5 under our experimental conditions. Further study is needed to refine this point.

Approaches using synthetic peptides and peptide libraries also implicated several segments of PrP^C in possible binding interfaces. For example, a peptide corresponding to residues 109 to 141 of hamster PrP was reported to inhibit the generation of a PK-resistant form of the PrP in an *in vitro* cell-free conversion assay (5). This led to speculation that the residues in the vicinity of positions 109 to 141 of either PrP^C or the PK-resistant form of PrP were involved in the intermolecular association (5). In screening assays utilizing MoPrP-derived peptide libraries grafted into immunoglobulin G molecules, the peptides corresponding to residues 23 to 33, 97 to 109, and 135 to 157 of MoPrP strongly bound to PrP^{Sc} (29, 30, 48). While peptide-based studies have demonstrated the putative binding interfaces between PrP^C and PrP^{Sc}, the antibodies against residues 143 to 151 (12), 143 to 153 (16), 132 to 156 and 220 to 231 (35), and 218 to 232 (18) of MoPrP or the amino acid substitution at residue 138 (37) interfered with the propagation of PrP^{Sc}. However, the incubation of prion-infected cells (RK13 cells) with the 1C5 antibody against residues 118 to 129 of MoPrP (7) for a week was ineffective at reducing the accumulation of PrP^{Sc} in the cells (16). We consider that the dominant and high-affinity binding interface for PrP^{Sc} is in the C-terminal half of PrP^C, as shown in Fig. 4B, and that these regions could be candidates for the initial binding interface between PrP^C and PrP^{Sc}.

It should be pointed out that the alanine-substituted mutants eliminated the endogenous PrP^{Sc} in ScN2a cells (Fig. 3B, bottom), while the mouse-chicken chimeras were unable to reduce the amounts of endogenous PrP^{Sc} (Fig. 2B, bottom). We reasoned that this was due to a difference in the affinity of the alanine-

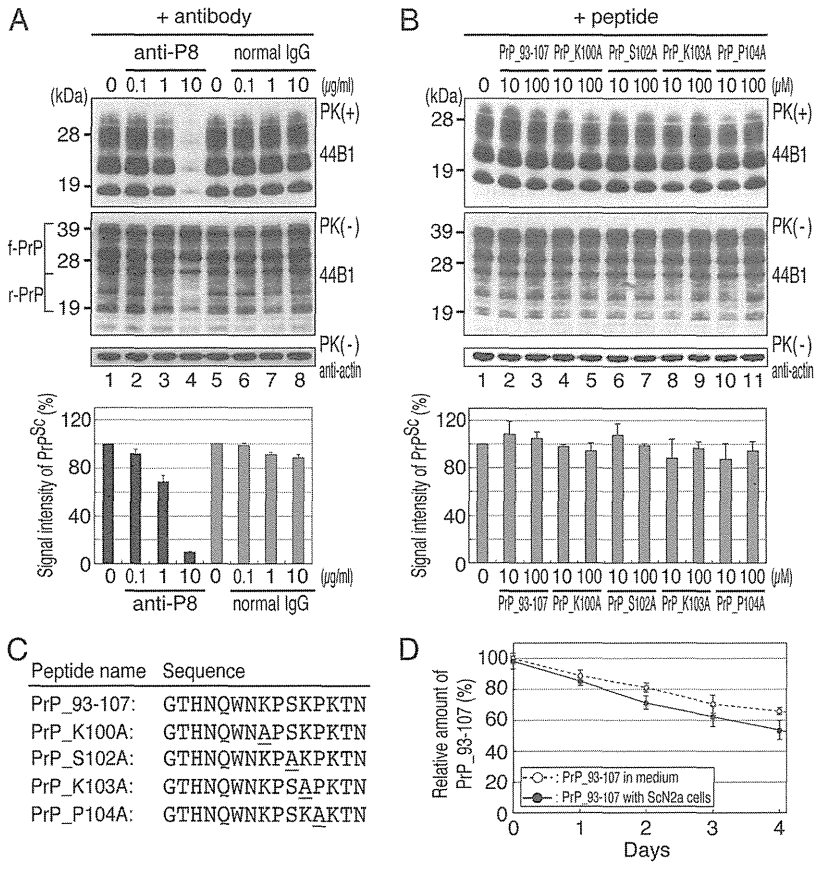

FIG 6 Anti-P8 antibody inhibits the accumulation of PrP^{Sc} in ScN2a cells, but a synthetic peptide derived from MoPrP residues 93 to 107 and its cognate peptides do not. (A) Western blot analysis of the lysate from ScN2a cells after 10 days of culture in the presence of the anti-P8 antibody or rabbit normal IgG at 0.1 to 10 μg/ml. PrP was detected by antibody 44B1. The lysate with PK digestion (top) shows the amount of PrP^{Sc}, and the lysate without digestion (middle) shows the total amount of PrP (i.e., PrP^{C} and PrP^{Sc}). The membrane was also probed with anti-actin antibody (bottom) for normalization of the protein content. The signal intensity of each PrP^{Sc} band detected in the upper membrane was quantified and expressed as a percentage of that in the absence of the antibody, with 0% denoting an undetectable level of PrP^{Sc} (invisible band). The data represent the means ± SEM for three independent experiments. (B) Western blot analysis of the lysate from ScN2a cells after 10 days of culture in the presence of the peptides at 10 or 100 μM. PrP was detected by antibody 44B1. The lysate with PK digestion (top) shows the amount of PrP^{Sc}, and the lysate without digestion (middle) shows the total amount of PrP (i.e., PrP^{C} and PrP^{Sc}). The membrane was also probed with the anti-actin antibody (bottom) for normalization of the protein content. The signal intensity of each PrP^{Sc} band detected in the upper membrane was quantified and expressed as a percentage of that in the absence of the peptides, with 0% denoting an undetectable level of PrP^{Sc} (invisible band). The data represent the means ± SEM for three independent experiments. (C) Sequences of peptides PrP_93-107, PrP_K100A, PrP_S102A, PrP_K103A, and PrP_P104A. The substituted alanine residues are underlined. (D) Time course of relative amounts of PrP_93-107 during the cell culture. The peptide was added to the medium with ScN2a cells (solid line) or without the cells (dashed line) at a concentration of 100 μM on day 0 and incubated at 37°C for up to 4 days. The amounts of PrP_93-107 were determined by reversed phase HPLC and are expressed as percent recovery. A 100% rating denotes no loss of PrP_93-107. The data represent means ± SEM for three independent experiments.

substituted mutants and the mouse-chicken chimeras for PrP^{Sc}, assuming that residues 95 to 104 serve as an auxiliary binding interface or in the coordination of the complex to strengthen the interaction between PrP^{C} and preexisting PrP^{Sc}. The single alanine substitution in the segment 100 to 104 (KPSKP) would not affect the affinity for preexisting PrP^{Sc} significantly, and the eventual "dead-end" complex hampered the growing amyloidotic assembly of PrP^{Sc} in the cells (Fig. 3B, bottom). The mouse-chicken chimeric PrPs, however, associated with preexisting PrP^{Sc} through their C-terminal regions (Fig. 4B, lanes 3 and 4), but the additional binding to or coordination with PrP^{Sc} was disrupted due to more than two amino acid mismatches between mouse and chicken sequences in the region of residues 95 to 104 of $MoPrP^{C}$. Thus, unlike the alanine-substituted mutants, the chimeras would be less stably associated with the preexisting PrP^{Sc} and, accordingly, incapable of competition and interference (Fig. 3B, bottom).

We found the replacement of Lys^{100}, Ser^{102}, Lys^{103}, or Pro^{104} in MoPrPs with Ala generated nonconvertible dead-end mutants. This finding, however, is inconsistent with a report that a MoPrP mutant in which the lysine residues at positions 100 and 103 were replaced with Ala was still converted to the PK-resistant form with an efficacy similar to that of the wild-type MoPrP in ScN2a cells (1). The reason for the discrepancy is unknown. In the above-mentioned report, the replacement of both Lys^{105} and Lys^{109} with Ala gave rise to a nonconvertible mutant, and the authors considered a PrP^{C}-PrP^{Sc}-interacting domain to be present between residues 106 and 110 of MoPrP (1).

Transgenic mice expressing a mutant MoPrP lacking residues 32 to 93 were shown to be susceptible to scrapie-prion agent,

though they showed a decrease in the deposition of PrP^{Sc} and no histopathological features of scrapie (13). In contrast, transgenic mice expressing a mutant MoPrP lacking residues 32 to 106 did not succumb to scrapie (14). These results suggest the functional importance of the segment examined in the present study. Recent studies using molecular fitting or molecular dynamics have predicted the amyloidotic assembly of PrP^{Sc} in trimeric, left-handed parallel β-helical folds (15, 43, 45, 49). The models predict that segment 100-KPSKP-104 of MoPrP forms an outward loop extending from the core β-helical architecture (15, 26, 49). Our results showing that the alanine substitutions at Lys^{100}, Ser^{102}, Lys^{103}, and Pro^{104} in MoPrP disrupted the conversion of PrP^C to PrP^{Sc} (Fig. 3) and that the replacement of the MoPrP sequence 95 to 98 (HNQW) with the corresponding chicken sequence (YHNQ) did not affect conversion efficacy (Fig. 2) highlight the functional importance of the predicted loop structure in the β-helical models.

In conclusion, segment 100 to 104 of MoPrP plays a critical role in promoting conversion. Also, while the primary binding interface seems to reside in the C-terminal region of PrP^C, this segment might be involved in the auxiliary binding interface of PrP^C to PrP^{Sc}. Further study is needed to clarify if the binding of the C-terminal region of PrP^C to PrP^{Sc} allosterically activates the segment 100 to 104 for conversion in the PrP^C-PrP^{Sc} complex.

ACKNOWLEDGMENTS

We thank M. Horiuchi (Hokkaido University) for the gift of the anti-PrP antibody 44B1 and K. Kaneko (Tokyo Medical University) for the cDNAs of MHM2 and MHM2-Q218K.

This work was supported by Grants-in-Aid for BSE Research from MHLW, Japan (H23-Shokuhin-Ippan-008).

REFERENCES

1. **Abalos GC, et al.** 2008. Identifying key components of the PrP^C-PrP^{Sc} replicative interface. J. Biol. Chem. **283**:34021–34028.
2. **Butler DA, et al.** 1988. Scrapie-infected murine neuroblastoma cells produce protease-resistant prion proteins. J. Virol. **62**:1558–1564.
3. **Calzolai L, Lysek DA, Pérez DR, Güntert P, Wüthrich K.** 2005. Prion protein NMR structures of chickens, turtles, and frogs. Proc. Natl. Acad. Sci. U. S. A. **102**:651–655.
4. **Caughey BW, et al.** 1991. Secondary structure analysis of the scrapie-associated protein PrP 27-30 in water by infrared spectroscopy. Biochemistry **30**:7672–7680.
5. **Chabry J, Caughey B, Chesebro B.** 1998. Specific inhibition of in vitro formation of protease-resistant prion protein by synthetic peptides. J. Biol. Chem. **273**:13203–13207.
6. **Chesebro B, et al.** 1985. Identification of scrapie prion protein-specific mRNA in scrapie-infected and uninfected brain. Nature **315**:331–333.
7. **Choi JK, et al.** 2006. Generation of monoclonal antibody recognized by the GXXXG motif (glycine zipper) of prion protein. Hybridoma **25**:271–277.
8. **DebBurman SK, Raymond GJ, Caughey B, Lindquist S.** 1997. Chaperone-supervised conversion of prion protein to its protease-resistant form. Proc. Natl. Acad. Sci. U. S. A. **94**:13938–13943.
9. **DeMarco ML, Daggett V.** 2004. From conversion to aggregation: protofibril formation of the prion protein. Proc. Natl. Acad. Sci. U. S. A. **101**:2293–2298.
10. **DeMarco ML, Silveira J, Caughey B, Daggett V.** 2006. Structural properties of prion protein protofibrils and fibrils: an experimental assessment of atomic models. Biochemistry **45**:15573–15582.
11. **Donne DG, et al.** 1997. Structure of the recombinant full-length hamster prion protein PrP(29-231): the N terminus is highly flexible. Proc. Natl. Acad. Sci. U. S. A. **94**:13452–13457.
12. **Enari M, Flechsig E, Weissmann C.** 2001. Scrapie prion protein accumulation by scrapie-infected neuroblastoma cells abrogated by exposure to a prion protein antibody. Proc. Natl. Acad. Sci. U. S. A. **98**:9295–9299.
13. **Flechsig E, et al.** 2000. Prion protein devoid of the octapeptide repeat region restores susceptibility to scrapie in PrP knockout mice. Neuron **27**:399–408.
14. **Flechsig E, Weissmann C.** 2004. The role of PrP in health and disease. Curr. Mol. Med. **4**:337–353.
15. **Govaerts C, Wille H, Prusiner SB, Cohen FE.** 2004. Evidence for assembly of prions with left-handed β-helices into trimers. Proc. Natl. Acad. Sci. U. S. A. **101**:8342–8347.
16. **Harrison CF, et al.** 2010. Conservation of a glycine-rich region in the prion protein is required for uptake of prion infectivity. J. Biol. Chem. **285**:20213–20223.
17. **Hetz C, Maundrell K, Soto C.** 2003. Is loss of function of the prion protein the cause of prion disorders? Trends. Mol. Med. **9**:237–243.
18. **Horiuchi M, Caughey B.** 1999. Specific binding of normal prion protein to the scrapie form via a localized domain initiates its conversion to the protease-resistant state. EMBO J. **18**:3193–3203.
19. **Horiuchi M, Priola SA, Chabry J, Caughey B.** 2000. Interactions between heterologous forms of prion protein: binding, inhibition of conversion, and species barriers. Proc. Natl. Acad. Sci. U. S. A. **97**:5836–5841.
20. **Hsiao K, et al.** 1989. Linkage of a prion protein missense variant to Gerstmann-Sträussler syndrome. Nature **338**:342–345.
21. **Kaneko K, et al.** 1997. Evidence for protein X binding to a discontinuous epitope on the cellular prion protein during scrapie prion propagation. Proc. Natl. Acad. Sci. U. S. A. **94**:10069–10074.
22. **Kim CL, et al.** 2004. Antigenic characterization of an abnormal isoform of prion protein using a new diverse panel of monoclonal antibodies. Virology **320**:40–51.
23. **Kishida H, et al.** 2004. Non-glycosylphosphatidylinositol (GPI)-anchored recombinant prion protein with dominant-negative mutation inhibits PrP^{Sc} replication *in vitro*. Amyloid **11**:14–20.
24. **Kitamoto T, et al.** 1993. A new inherited prion disease (PrP-P105L mutation) showing spastic paraparesis. Ann. Neurol. **34**:808–813.
25. **Kong Q, et al.** 2004. Inherited prion diseases, p 673–775. *In* Prusiner SB (ed), Prion biology and diseases, 2nd ed. Cold Spring Harbor Laboratory Press, Cold Spring Harbor, NY.
26. **Kunes KC, Clark SC, Cox DL, Singh RR.** 2008. Left handed β helix models for mammalian prion fibrils. Prion **2**:81–90.
27. **Leclerc E, et al.** 2001. Immobilized prion protein undergoes spontaneous rearrangement to a conformation having features in common with the infectious form. EMBO J. **20**:1547–1554.
28. **Lund C, Olsen CM, Tveit H, Tranulis MA.** 2007. Characterization of the prion protein 3F4 epitope and its use as a molecular tag. J. Neurosci. Methods **165**:183–190.
29. **Moroncini G, et al.** 2004. Motif-grafted antibodies containing the replicative interface of cellular PrP are specific for PrP^{Sc}. Proc. Natl. Acad. Sci. U. S. A. **101**:10404–10409.
30. **Moroncini G, et al.** 2006. Pathologic prion protein is specifically recognized in situ by a novel PrP conformational antibody. Neurobiol. Dis. **23**:717–724.
31. **Nelson R, et al.** 2005. Structure of the cross-β spine of amyloid-like fibrils. Nature **435**:773–778.
32. **Oesch B, et al.** 1985. A cellular gene encodes scrapie PrP 27-30 protein. Cell **40**:735–746.
33. **Okemoto-Nakamura Y, et al.** 2008. Synthetic fibril peptide promotes clearance of scrapie prion protein by lysosomal degradation. Microbiol. Immunol. **52**:357–365.
34. **Peretz D, et al.** 1997. A conformational transition at the N terminus of the prion protein features in formation of the scrapie isoform. J. Mol. Biol. **273**:614–622.
35. **Peretz D, et al.** 2001. Antibodies inhibit prion propagation and clear cultures of prion infectivity. Nature **412**:739–743.
36. **Premzl M, Gamulin V.** 2007. Comparative genomic analysis of prion genes. BMC Genomics **8**:1.
37. **Priola SA, Chesebro B.** 1995. A single hamster PrP amino acid blocks conversion to protease-resistant PrP in scrapie-infected mouse neuroblastoma cells. J. Virol. **69**:7754–7758.
38. **Priola SA, Lawson VA.** 2001. Glycosylation influences cross-species formation of protease-resistant prion protein. EMBO J. **20**:6692–6699.
39. **Prusiner SB.** 1982. Novel proteinaceous infectious particles cause scrapie. Science **216**:136–144.
40. **Prusiner SB, Groth DF, Bolton DC, Kent SB, Hood LE.** 1984. Purification and structural studies of a major scrapie prion protein. Cell **38**:127–134.

41. **Prusiner SB.** 2004. Prion biology and diseases, 2nd ed. Cold Spring Harbor Laboratory Press, Cold Spring Harbor, NY.
42. **Riek R, Hornemann S, Wider G, Glockshuber R, Wüthrich K.** 1997. NMR characterization of the full-length recombinant murine prion protein, mPrP(23-231). FEBS Lett. **413**:282–288.
43. **Sajnani G, Pastrana MA, Dynin I, Onisko B, Requena JR.** 2008. Scrapie prion protein structural constraints obtained by limited proteolysis and mass spectrometry. J. Mol. Biol. **382**:88–98.
44. **Sakudo A, et al.** 2003. Absence of superoxide dismutase activity in a soluble cellular isoform of prion protein produced by baculovirus expression system. Biochem. Biophys. Res. Commun. **307**:678–683.
45. **Samson AO, Levitt M.** 2011. Normal modes of prion proteins: from native to infectious particle. Biochemistry **50**:2243–2248.
46. **Scheibel T, Bloom J, Lindquist SL.** 2004. The elongation of yeast prion fibers involves separable steps of association and conversion. Proc. Natl. Acad. Sci. U. S. A. **101**:2287–2292.
47. **Scott MR, Köhler R, Foster D, Prusiner SB.** 1992. Chimeric prion protein expression in cultured cells and transgenic mice. Protein Sci. 1:986–997.
48. **Solforosi L, et al.** 2007. Toward molecular dissection of PrP^{C}-PrP^{Sc} interactions. J. Biol. Chem. **282**:7465–7471.
49. **Stork M, Giese A, Kretzschmar HA, Tavan P.** 2005. Molecular dynamics simulations indicate a possible role of parallel β-helices in seeded aggregation of poly-Gln. Biophys. J. **88**:2442–2451.
50. **Taraboulos A, Serban D, Prusiner SB.** 1990. Scrapie prion proteins accumulate in the cytoplasm of persistently infected cultured cells. J. Cell Biol. **110**:2117–2132.
51. **Veith NM, Plattner H, Stuermer CA, Schulz-Schaeffer WJ, Bürkle A.** 2009. Immunolocalisation of PrP^{Sc} in scrapie-infected N2a mouse neuroblastoma cells by light and electron microscopy. Eur. J. Cell Biol. **88**:45–63.
52. **Wille H, et al.** 2002. Structural studies of the scrapie prion protein by electron crystallography. Proc. Natl. Acad. Sci. U. S. A. **99**:3563–3568.
53. **Williamson RA, et al.** 1998. Mapping the prion protein using recombinant antibodies. J. Virol. **72**:9413–9418.
54. **Yamada M, et al.** 1993. A missense mutation at codon 105 with codon 129 polymorphism of the prion protein gene in a new variant of Gerstmann-Sträussler-Scheinker disease. Neurology **43**:2723–2724.

J. Biochem. 2013;153(2):139–145 doi:10.1093/jb/mvs148

JB THE JOURNAL OF BIOCHEMISTRY

JB Review

Species-barrier phenomenon in prion transmissibility from a viewpoint of protein science

Received October 4, 2012; accepted November 29, 2012; published online January 2, 2013

Ken'ichi Hagiwara*, Hideyuki Hara† and Kentaro Hanada

Department of Biochemistry and Cell Biology, National Institute of Infectious Diseases, Tokyo 162-8640, Japan

*Ken'ichi Hagiwara, Department of Biochemistry and Cell Biology, National Institute of Infectious Diseases, 1-23-1 Toyama, Shinjuku-ku, Tokyo 162-8640. Tel: 81-3-4582-2734, Fax: 81-3-5285-1157, email: hagiwark@nih.go.jp

†Present address: Hideyuki Hara, BioResource Room, The Institute for Enzyme Research, The University of Tokushima, 3-18-15 Kuramoto-cho, Tokushima city, Tokushima 770-8503, Japan.

Transmissible spongiform encephalopathies (TSEs), or prion diseases, are fatal infectious neurodegenerative disorders. Their causative agents are prions, which are composed of disease-associated forms of prion protein (PrP^{Sc}). Naturally occurring cases of TSEs are found in several mammalian species including humans, sheep, goats, minks, cattle and deer. Prions are also experimentally transmissible to other mammals such as mice, hamsters and monkeys, but interspecies transmission is often inefficient due to the 'species-barrier'. Studies have suggested that the barrier is not only simply determined by differences in amino acid sequences of cellular PrP (PrP^{C}) among animal species, but also by prion strains which are closely associated with conformational properties of PrP^{Sc} aggregates. Although the conformational properties of PrP^{Sc} remain largely unknown, recent investigation of local structures of PrP^{C} and, in particular, structural modelling of PrP^{Sc} aggregates have provided molecular insight into this field. In this review, we discuss the species-barrier phenomenon in terms of the protein science.

Keywords: amyloid/left-handed parallel β-helix/prion/species-barrier/spiral model.

Abbreviations: BSE, bovine spongiform encephalopathy; CJD, Creutzfeldt–Jakob disease; C-terminal, carboxyl-terminal; CWD, chronic wasting disease; NMR, nuclear magnetic resonance; N-terminal, amino-terminal; PrP, prion protein; PrP^{C}, cellular PrP; PrP^{Sc}, disease-associated forms of PrP; TSEs, transmissible spongiform encephalopathies; vCJD, variant CJD.

Transmissible spongiform encephalopathies (TSEs), or prion diseases, are fatal neurodegenerative disorders. The diseases are typically characterized by neuronal cell loss and vacuolation in the central nervous system (*1*). Human prion diseases are etiologically found as sporadic, inherited or acquired (*i.e.* infected) cases, and include Creutzfeldt–Jakob disease (CJD), Gerstmann–Sträussler–Scheinker syndrome, fatal familial insomnia, iatrogenic CJD, variant CJD (vCJD) and kuru. Not only in acquired cases but also in sporadic and inherited cases, tissues of neuropathological lesions usually exhibit infectivity. TSEs are found also in sheep and goats as scrapie, in minks as transmissible mink encephalopathy, in cattle as bovine spongiform encephalopathy (BSE) and in deer as chronic wasting disease (CWD). The infectious agents causative of TSEs are quite different from conventional microbes such as bacteria and viruses (*2*), and are termed 'prions' denoting the peculiarity of the agent; a *pro*teinaceous *in*fectious particle (*1*, *3*). Currently, the prion entity is conceived to be disease-associated forms of prion protein (PrP^{Sc}; PrP refers to prion protein), which are conformational isoforms of the cellular PrP (PrP^{C}) encoded by the host gene (*4*, *5*).

The amino acid sequences of PrP^{C} are highly conserved in mammalian species. Mouse PrP^{C} consists of 254 amino acids including a signal peptide at the amino-terminus (N-terminus) for targeting the endoplasmic reticulum (ER) membrane lumen, a signal peptide at the carboxyl-terminus (C-terminus) for addition of a glycosylphosphatidylinositol-anchor, and two asparagines for *N*-glycosylation (*6*). The physiological functions of PrP^{C} remain unknown, but it is proposed to be involved in cell-to-cell recognition, signal transduction by coupling with certain transmembrane-type receptors, the response to oxidative stress, or the uptake of metal ions into cells (reviewed in Ref. *7*).

Seed-Dependent Conformational Conversion of PrP^{C} to PrP^{Sc}

Propagation of PrP^{Sc} takes place through a catalytic conversion of PrP^{C} to PrP^{Sc} by binding of PrP^{C} to pre-existing PrP^{Sc} seeds (*8*), though it is unclear how the initial PrP^{Sc} seeds are generated in TSEs other than the acquired cases. The replicative propagation of PrP^{Sc} produces protofibrils, which elongate subsequently into amyloid fibrils. In living cells, such seed-dependent conversion takes place in lipid rafts of the plasma membrane and/or in the early endocytic pathway (*9*), and prions spread spatially to nearby cells by cell-to-cell contact and by release of microvesicles containing PrP^{Sc} (*10–12*). The two *N*-glycans of PrP^{C} are not mandatory for the conversion of PrP^{C} to PrP^{Sc} (*13*, *14*).

In operational criteria, PrP^{Sc} can be distinguished from PrP^{C} by its resistance to proteolytic digestion by proteinase K (*15*). Although PrP^{C} is susceptible to digestion by proteinase K, PrP^{Sc} is partially resistant to

the digestion and its carboxyl-terminal (C-terminal) half remains undegraded. Mass spectrometric analysis of PrP^{Sc} derived from the brain of scrapie-affected sheep showed that the undegraded C-terminal half started mostly from residues 85–94 of the sheep PrP amino acid sequence (corresponding to residues 81–89 in mouse PrP) (*16*).

Infrared spectroscopy showed PrP^{C} to have a high α-helix content (42%) (*17*). In contrast, the analysis suggested that PrP^{Sc} after proteinase K-digestion is more abundant in β-sheets (54%) than α-helices (21%) (*17*), or β-sheets (47%) and turns (31%) than α-helices (17%) (*18*). A high β-sheet content is consistent with the amyloidogenic properties of PrP^{Sc}.

Species-Barrier of Prions

Although the transmission of prions within the same mammalian species is efficient, that between different species is usually affected by the 'species-barrier'. The species-barrier gives rise to infrequent transmission and prolonged incubation periods prior to neurodegenerative onset after the inoculation of prions. It is occasionally of sufficient magnitude to substantially block transmission, or to prevent many of the inoculated animals from developing the disease during their lifetime (*19*). However, the barrier sometimes can be negligible depending on the combination of donor and recipient animals. For instance, scrapie prion is epidemiologically believed not to be transmissible to humans, but lines of evidence indicate that BSE prion is transmissible to humans and is responsible for the emergence of vCJD (*20*, *21*).

As expected from the seed-dependent conversion of PrP^{C} to PrP^{Sc}, differences in the amino acid sequences of PrP in donor and recipient animals are a strong constraint to the species-barrier. However, the species-barrier cannot simply be explained by mismatches in the amino acid sequences of PrP. For example, even though prions derived from patients with sporadic CJD and vCJD are invariably composed of PrP^{Sc} with the human amino acid sequence, sporadic CJD prion was hardly transmissible to inbred FVB mice while vCJD prion was transmissible to these mice (*21*). The situation is also remarkable for prion strains of classical BSE and atypical BSE (so called L-BSE) (*22*, *23*), which are equally composed of PrP^{Sc} of the bovine amino acid sequence. Classical BSE prion was transmissible to inbred mice and caused the disease, whereas atypical BSE prion did not (*24*, *25*). On the other hand, cross-species transmission of atypical L-BSE prion to crab-eating macaque monkeys (*Macaca fascicularis*) was accomplished in shorter incubation periods than that of classical BSE prion to the monkeys (*26*, *27*). It was also reported that the cross-species transmission of L-BSE prion to Syrian hamsters (*Mesocricetus auratus*) was more efficient than that of classical BSE prion (*28*).

From these studies, we are increasingly realizing that the species-barrier is closely related to the properties of prion strains, and strains should be defined by local conformations of PrP^{C}, or conformations of PrP^{Sc} aggregates. It remains mostly unsolved how conformational properties participate in the species-barrier, but recent structural analyses have provided intriguing insights that we discuss in the following sections.

Consideration for the Species-Barrier Based on the Structures of PrP^{C}

Nuclear magnetic resonance (NMR) studies of mammalian recombinant PrPs (*29–33*) showed that the amino-terminal (N-terminal) half is flexible, whereas the C-terminal half (residues 121–231 in the mouse sequence) consists of three α-helices (helices A, B and C) and two anti-parallel β-sheets (Fig. 1). The central positions of helices B and C form relatively rigid cores, and the two anti-parallel β-sheets and connecting loops are moderately flexible (*33*). Such features most likely reflect the structure of PrP^{C}. Interestingly, the structural fold of chicken (*Gallus gallus*), turtle (*Trachemys scripta*) and frog (*Xenopus laevis*) recombinant PrPs is very similar to that of mammalian PrPs (*34*), despite limited amino acid sequence homology.

Despite the similar overall structure of PrP^{C} in different animal species, comparison of the NMR structures of recombinant mammalian PrPs indicated conformational variability in the second β-sheet and helix B (*32*, *35*) (β2-α2 loop, Fig. 1). Gossert *et al.* (*35*) argued that the variability of the β2-α2 loop was ascribable to the amino acids at positions 169 and 173 in the loop [mouse numbering; Ser^{169}/Asn^{173} for humans, mice, sheep and cows, Asn^{169}/Asn^{173} for Syrian hamsters, and Asn^{169}/Thr^{173} for elk (*Cervus elaphus nelsoni*)]. They expected the β2-α2 loop having Ser^{169}/Asn^{173} to exhibit a wobbling conformation and the loop with Asn^{169}/Thr^{173} to have a rigid conformation (*35*). Based on this notion, Sigurdson *et al.* (*37*) generated two lines of transgenic mice

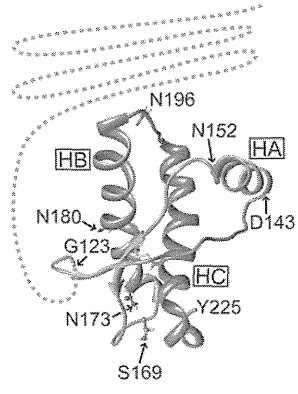

Fig. 1 NMR Structure of mouse recombinant PrP. The three α-helices A, B and C (HA spanning from D^{143} to N^{152}, HB and HC) are coloured blue, two anti-parallel β-sheets are green and the N-terminal flexible part (residues 23–122) is shown with dotted lines. The β2-α2 loop (containing S^{169} and N^{173}) is shown in orange. N^{180} and N^{196} are potential glycosylation sites. The image was produced using the data in the Protein Data Bank (PDB ID: 1AG2) (*29*) and the UCSF Chimera package from the Resource for Biocomputing, Visualization, and Informatics at the University of California, San Francisco, CA (*36*).

overexpressing either wild-type mouse PrP^C (Ser^{169}/Asn^{173}; a wobble loop) or mutant mouse PrP^C (Asn^{169}/Thr^{173}; a rigid loop). Inoculation of these mice with prions from different sources (scrapie prion from sheep, BSE prion from cows, CWD prion from elk and scrapie prions passaged in mice or hamsters) showed that prions propagated from Ser^{169} templates (*i.e.* prions from sheep, mouse and cow) are poorly transmissible to the recipient mice with the rigid loop (Asn^{169}/Thr^{173}) and, conversely, prions propagated from Asn^{169} templates (*i.e.* prions from hamsters and elk) are poorly transmissible to the recipient mice with the wobbling loop (Ser^{169}/Asn^{173}) (*37*). This suggests that the structural plasticity of the β2-α2 loop (*32*, *35*) is conducive to the species-barrier phenomenon.

Left-Handed Parallel β-Helical Models of PrP^{Sc} Aggregates

Structural analysis of PrP^{Sc} is challenging because of the technical incompatibility of the insoluble PrP^{Sc} aggregates with NMR spectroscopy or X-ray crystallography. However, a breakthrough was made recently using electron microscopic images of isomorphous crystals found in amyloid fibrils of PrP^{Sc} (*38*). Two-dimensional projection maps at a resolution of 7 Å from the electron microscopic images suggested that the conversion of PrP^C to PrP^{Sc} accompanied transformation of the N-terminal part of PrP^C into a triangular left-handed or right-handed parallel β-helical fold, with most of helices B and C remaining intact (*38*). This model was further refined to show the N-terminal half of PrP^{Sc} folding into four-rung left-handed parallel β-helices, and two extra loops consisting of Lys^{100}–Pro^{104} and Glu^{145}–Arg^{163} (mouse numbering) (Fig. 2B, left) (*39*). In the model, PrP^{Sc} assembles into planar trimers by facing the triangular β-helices, and the trimers stack along the axis as a fibril (Fig. 3B). Helices B and C, and the two *N*-linked glycans are supposed to be on the periphery of the oligomers (*38*, *39*). The β2-α2 loop (*32*, *35*, *37*) described in the previous section was transformed to a part of rung-4 in the β-helical fold (Fig. 2B, left).

The basic architecture of the left-handed parallel β-helical fold is exemplified by UDP-*N*-acetylglucosamine acyltransferase from *Escherichia coli* (LpxA, PDB ID: 1LXA) (Fig. 2A) (*40*). Each triangular rung is typically composed of three hexapeptides (*t1*, *t2*, *b1*, *b2*, *b3* and *b4* in Fig. 2B, top left), and irregular insertions of loops of various lengths. The side chains of amino acids at turns (*t1* and *t2*) and at the fourth and sixth positions (*b2* and *b4*) are oriented outward and participate in interoligomer interaction, whereas the side chains at the third and fifth positions (*b1* and *b3*) face inward to fill the central core of the β-helix.

The PrP^{Sc} models as described earlier (*38*, *39*) prompted molecular dynamics simulations to predict divergent models of left-handed parallel β-helices (*41–43*). Langedijk *et al.* (*42*) posed a two-rung model in which Met^{109} and Met^{129} in the two adjacent rungs form a sulphur stack (Fig. 2B, middle), based on the notion that the sulphur stack explains the species-barrier between mice and hamsters. The helices B and C in the two-rung model (*42*) are supposed to remain intact as in the four-rung model (*38*, *39*). Although this model (*i.e.* two-rungs of β-sheets per monomer) seems to contradict the infrared spectroscopic data which suggested a high β-sheet content in PrP^{Sc} (*17*, *18*), Langedijk *et al.* (*42*) pointed out the possibility that the β-sheet content was overestimated in the infrared spectroscopic analysis due to hydrogen bonds at the turns and loops in the β-helical rungs. Another model, an N+C model, is distinguished from the others because both the N- and the C-terminal halves of PrP^{Sc} fold into left-handed parallel β-helices (Fig. 2B, right) (*43*). Regarding the intramolecular disulphide-bond between Cys^{178} and Cys^{213} (mouse numbering) in the C-terminal part of PrP^C, the N+C model had no difficulty accommodating it during the conformational conversion of PrP^C to PrP^{Sc} by placing the two half cystines at triangular corners of the adjacent rungs of the β-helical fold (Fig. 2B, right) (*43*).

These theoretical PrP^{Sc} models are interesting, but is it feasible for the N-terminal part of PrP^{Sc} to fold into left-handed parallel β-helices? To answer this fundamental question, rung-2, −3 and −4 of the *E. coli* LpxA protein were replaced by the N-terminal part of the mouse PrP segment (amino acid residues 104–143). The chimera LpxA exhibited similar levels of enzyme activity to wild-type LpxA, supporting the notion that the mouse PrP 104–143 segment potentially folds into a β-helical structure (*44*).

Consideration of Species-Barrier from Left-Handed Parallel β-Helical Models

Figure 2B shows the putative allocation of amino acid residues in the left-handed parallel β-helical models. The amino acids are shown in colours to indicate the differences between human–sheep (yellow), mouse–Syrian hamster (blue), or both human–sheep and mouse–Syrian hamster (magenta), in light of the well-known species-barrier for scrapie prion between humans and sheep, and between mice and Syrian hamsters. At the moment, we cannot predict determinants for the species-barrier from these diagrams. However, spatial proximity of species-dependent inward-facing residues is worth noticing, such as Leu^{108} and Val^{111} (mice versus hamsters) or Val^{165} and Gln^{167} (humans versus sheep) in the four-rung model (Fig. 2B, left), or Leu^{108} and Ile^{138} (mice versus hamster) in the N+C model (Fig. 2B, right). This seems to have implications for the species-barrier, because the side chains of the inward-facing residues fill the core of the β-helix, and their species-dependent clusters may affect subtle architectural changes of a triangular structure of the helix (*41*, *42*).

Recently, Hara *et al.* (*45*) showed that the mouse PrP segment 95–98 (HNQW) could be replaced with the corresponding chick segment (YHNQ) without a loss of conversion to PrP^{Sc} in prion-infected mouse neuroblastoma cells. If the four-rung model is accurate

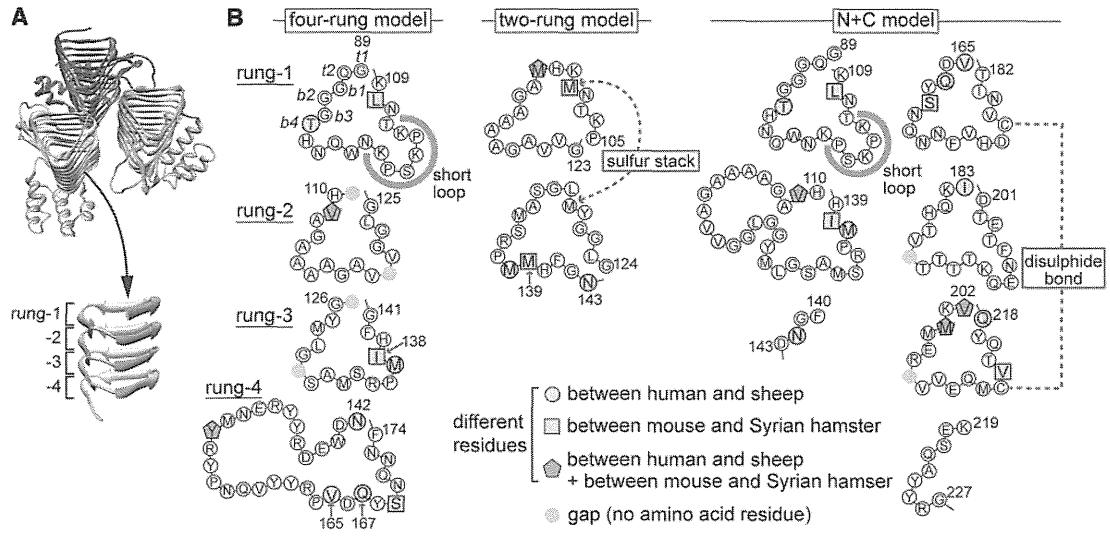

Fig. 2 Left-handed parallel β-helical models. (A) X-ray crystal structure of UDP-*N*-acetylglucosamine acyltransferase from *Escherichia coli* (LpxA, PDB ID: 1LXA) (*40*). The image was produced using the UCSF Chimera package (*36*). (B) Putative allocation of amino acid residues in the left-handed parallel β-helices of PrP^{Sc} summarized from the original data (*39*, *42*, *43*). Amino acid residues in the four-rung model (*39*) and the N+C model (represents N2 and C4D conformers in the original paper) (*43*) are numbered according to the mouse PrP sequence, whereas the two-rung model (*42*) is numbered based on Syrian hamster PrP to emphasize the hamster-specific sulphur stack of methionines. The letter *t* denotes residues at turns, and the letter *b* denotes residues in β-sheets. Amino acids are shown in colours to indicate the difference between human–sheep (yellow), mouse–hamster (blue), and both human–sheep and mouse–hamster (magenta).

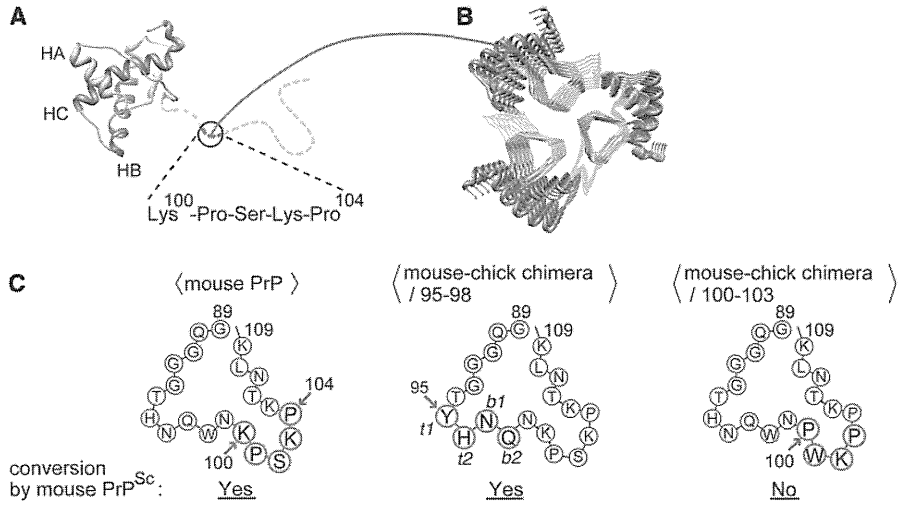

Fig. 3 The loop structure in left-handed parallel β-helical models of PrP^{Sc}. (A) NMR structure of mouse recombinant PrP (PDB ID: 1AG2) (*29*). (B) The four-rung left-handed parallel β-helical model of PrP^{Sc} (*39*) in which the yellow region in (A) is converted to β-helices. Note that residues 100 to 104 in the flexible region of mouse recombinant PrP shown in (A) (*30*, *32*, *33*) are presumed to form a loop (shown in red) in the PrP^{Sc} model. The image was produced based on the structure of LpxA (PDB ID: 1LXA) (*40*) with adaptations of the images of the four-rung model reported (*39*), and by using the UCSF Chimera package (*36*). (C) Allocation of amino acid residues of mouse PrP^{Sc} (left) according to the four-rung model (*39*), and putative allocation of amino acid residues of mouse-chick chimeric PrPs (middle and right), with the results of a conversion study in prion-infected neuroblastoma cells (*45*).

in the mouse-chick chimeric PrP, residues 95–98 are at the positions *t1*, *t2*, *b1* and *b2* in the top rung (Fig. 3C, middle). The results indicate that positions *t1*, *t2*, *b1* and *b2* in the top rung do not participate in the conversion process and, possibly, in species-barrier. In contrast, the mouse PrP sequence Lys^{100}–Lys^{103} (KPSK) is vital. Replacement of this sequence with the corresponding chick sequence (PWKP) (Fig. 3C, right), or alanine-substitutions at Lys^{100}, Ser^{102}, Lys^{103} or Pro^{104} impaired conversion of the chimera (*45*).

It should be noted that the region Lys^{100}–Lys^{104} (KPSKP) is conformationally flexible in PrP^{C} (Fig. 3A) (*30*, *32*, *33*), but forms a short loop on the top rung in the β-helix models of PrP^{Sc} (Fig. 2B, the four-rung and N+C models; Fig. 3A and B, shown in red) (*39*, *43*). Taking into account the recent finding

that soluble proteins of the β-helix motif family have 'cap' structures on each end of the β-helices to prevent self-aggregation (*46*), the short Lys^{100}–Lys^{104} loop could play the opposite role as a 'sticky-string' to facilitate adhesion of the top rung to the bottom of the next layer of β-helices. However, this possibility seems unlikely, because excess amounts of synthetic peptides with this loop region did not competitively block the conversion of PrP^C to PrP^{Sc} (*45*).

Spiral Model and Steric Zipper Model of PrP^{Sc} Aggregates

Another model of PrP^{Sc} is a spiral model (*47*, *48*). The model was based on molecular dynamics simulations of a NMR structure of recombinant Syrian hamster PrP (PDB ID: 1B10). In the spiral model, residues 116–132 and 160–164 (Syrian hamster numbering) transform into three β-sheets to build a spiralling core. Trimeric assembly of the spiral model seems more favourable than the β-helix models for accommodation of the glycan moieties in the fibril structures (*48*). Different from the four-rung left-handed parallel β-helices in which helix A of PrP^C is converted to a part of loop in rung-4 (Fig. 2B, left) (*38*, *39*), helix A (from Asp^{144} to Asn^{153} in the Syrian hamster numbering) remains intact in the spiral model (*47*, *48*). The β2-α2 loop of PrP^C (*32*, *33*, *35*, *37*) is buried in the trimer of the spiralling core (*49*).

It was shown previously that Ile^{138} of mouse PrP (corresponding to Met^{139} of hamster PrP) is one of key residues for the species-barrier between mice and hamsters (*50*), and Ile^{138} is assumed to be inward-facing residues in the rung models (Fig. 2B, see the four-rung and the N+C models for mouse Ile^{138}; the two-rung model for hamster Met^{139}) (*39*, *42*, *43*). To gain structural insight into this residue, a synthetic peptide composed of mouse PrP residues 137 to 142, and peptides corresponding to the Syrian hamster and human sequences were subjected to analysis by X-ray crystallography. The mouse and human peptides formed parallel steric zippers in the crystals, and the residues of two neighbouring β-sheet layers were tightly interdigitated. In contrast, the hamster peptide formed anti-parallel zippers (*51*). Such dissimilar zipper structures might give rise to transmission barriers (*51*). Whether these zipper structures are adaptable to the β-helical and/or spiral models remains to be examined, but a recent study using computational simulation proposed a new model of PrP^{Sc} having zipper structures (*52*).

Conclusion and Perspectives

Differences in amino acid sequences of PrP in donor and recipient animals are a constraint on the species-barrier to the transmissibility of prions. In addition, it has now become apparent that the barrier can be crossed if the conformational properties of PrP^{Sc} and plasticity of PrP^C have the capacity to compromise the mismatches of amino acid sequences. In this regard, recent X-ray diffraction data for PrP^{Sc} suggested the existence of structures other than the four-rung left-handed parallel β-helices (*53*), and it is now conceivable that prion populations constitute 'quasispecies'; the most efficiently replicating variant represents the strain, but one of the coexisting minor conformational variants becomes dominant if the environment changes (reviewed in Ref. *54*). So, the distinct PrP^{Sc} models proposed to date might be snapshots of potential forms of prion variants. Modelling of PrP^{Sc} structures is thus further encouraged.

Funding
Grants-in-aid for BSE Research from MHLW, Japan (H23-Shokuhin-Ippan-005) (to K.H.).

Conflict of Interest
None declared.

References

1. Prusiner, S.B. (2004) *Prion Biology and Disease*. 2nd edn. Cold Spring Harbor Laboratory Press, Cold Spring Harbor, NY
2. Alper, T., Cramp, W.A., Haig, D.A., and Clarke, M.C. (1967) Does the agent of scrapie replicate without nucleic acid? *Nature* **214**, 764–766
3. Prusiner, S.B. (1982) Novel proteinaceous infectious particles cause scrapie. *Science* **216**, 136–144
4. Chesebro, B., Race, R., Wehrly, K., Nishio, J., Bloom, M., Lechner, D., Berbstrom, S., Robbins, K., Mayer, L., Keith, J.M., Garon, C., and Hasse, A. (1985) Identification of scrapie prion protein-specific mRNA in scrapie-infected and uninfected brain. *Nature* **315**, 331–333
5. Stahl, N., Baldwin, M.A., Teplow, D.B., Hood, L., Gibson, B.W., Burlingame, A.L., and Prusiner, S.B. (1993) Structural studies of the scrapie prion protein using mass spectrometry and amino acid sequencing. *Biochemistry* **32**, 1991–2002
6. Rudd, P.M., Endo, T., Colominas, C., Groth, D., Wheeler, S.F., Harvey, D.J., Wormald, M.R., Serban, H., Prusiner, S.B., Kobata, A., and Dwek, R.A. (1999) Glycosylation differences between the normal and pathogenic prion protein isoforms. *Proc. Natl. Acad. Sci. U S A.* **96**, 13044–13049
7. Linden, R., Martins, V.R., Prado, M.A.M., Cammarota, M., Izquierdo, I., and Brentani, R.R. (2008) Physiology of the prion protein (Review). *Physiol. Rev.* **88**, 673–728
8. Horiuchi, M, Priola, S.A., Chabry, J., and Caughey, B. (2000) Interactions between heterologous forms of prion protein: binding, inhibition of conversion, and species barriers. *Proc. Natl. Acad. Sci. U S A.* **97**, 5836–5841
9. Veith, N.M., Plattner, H., Stuermer, C.A.O., Schulz-Schaeffer, W.J., and Bürkle, A. (2009) Immunolocalisation of PrP^{Sc} in scrapie-infected N2a mouse neuroblastoma cells by light and electron microscopy. *Eur. J. Cell Biol.* **88**, 45–63
10. Fevrier, B., Vilette, D., Archer, F., Loew, D., Faigle, W., Vidal, M., Laude, H., and Raposo, G. (2004) Cells release prions in association with exosomes. *Proc. Natl. Acad. Sci. U S A.* **101**, 9683–9688
11. Paquet, S., Langevin, C., Chapuis, J., Jackson, G.S., Laude, H., and Vilette, D. (2007) Efficient dissemination of prions through preferential transmission to nearby cells. *J. Gen. Virol.* **88**, 706–713

12. Tanaka, M., Hara, H., Nishina, H., Hanada, K., Hagiwara, K., and Maehama, T. (2010) An improved method for cell-to-cell transmission of infectious prion. *Biochem. Biophys. Res. Commun.* **397**, 505–508
13. Neuendorf, E., Weber, A., Saalmueller, A., Schatzl, H., Reifenberg, K., Pfaff, E., and Groschup, M.H. (2004) Glycosylation deficiency at either one of the two glycan attachment sites of cellular prion protein preserves susceptibility to bovine spongiform encephalopathy and scrapie infections. *J. Biol. Chem.* **279**, 53306–53316
14. Tuzi, N.L., Cancellotti, E., Baybutt, H., Blackford, L., Bradford, B., Plinston, C., Coghill, A., Hart, P., Piccardo, P., Barron, R.M., and Manson, J.C. (2008) Host PrP glycosylation: a major factor determining the outcome of prion infection. *PLoS Biol.* **6**, e100
15. Serban, D., Taraboulos, A., DeArmond, S.J., and Prusiner, S.B. (1990) Rapid detection of Creutzfeldt-Jakob disease and scrapie prion proteins. *Neurology* **40**, 110–117
16. Gielbert, A., Davis, L.A., Sayers, A.R., Hope, J., Gill, A.C., and Sauer, M.J. (2009) High-resolution differentiation of transmissible spongiform encephalopathy strains by quantitative N-terminal amino acid profiling (N-TAAP) of PK-digested abnormal prion protein. *J. Mass Spectrom.* **44**, 384–396
17. Pan, K.M., Baldwin, M., Nguyen, J., Gasset, M., Serban, A., Groth, D., Mehlhorn, I., Huang, Z., Fletterick, R.J., Cohen, F.E., and Prusiner, S.B. (1993) Conversion of α-helices into β-sheets features in the formation of the scrapie prion proteins. *Proc. Natl. Acad. Sci. U S A.* **90**, 10962–10966
18. Caughey, B.W., Dong, A., Bhat, K.S., Ernst, D., Hayes, S.F., and Caughey, W.S. (1991) Secondary structure analysis of the scrapie-associated protein PrP 27-30 in water by infrared spectroscopy. *Biochemistry* **30**, 7672–7680
19. Hill, A.F., Joiner, S., Linehan, J., Desbruslais, M., Lantos, P.L., and Collinge, J. (2000) Species-barrier-independent prion replication in apparently resistant species. *Proc. Natl. Acad. Sci. U S A.* **97**, 10248–10253
20. Bruce, M.E., Will, R.G., Ironside, J.W., McConnell, I., Drummond, D., Suttie, A., McCardle, L., Chree, A., Hope, J., Birkett, C., Cousens, S., Fraser, H., and Bostock, C.J. (1997) Transmissions to mice indicate that 'new variant' CJD is caused by the BSE agent. *Nature* **389**, 498–501
21. Hill, A.F., Desbruslais, M., Joiner, S., Sidle, K.C.L., Gowland, I., Collinge, J., Doey, L.J., and Lantos, P. (1997) The same prion strain causes vCJD and BSE. *Nature* **389**, 448–450
22. Casalone, C., Zanusso, G., Acutis, P., Ferrari, S., Capucci, L., Tagliavini, F., Monaco, S., and Caramelli, M. (2004) Identification of a second bovine amyloidotic spongiform encephalopathy: Molecular similarities with sporadic Creutzfeldt-Jakob disease. *Proc. Natl. Acad. Sci. U S A.* **101**, 3065–3070
23. Hagiwara, K., Yamakawa, Y., Sato, Y., Nakamura, Y., Tobiume, M., Shinagawa, M., and Sata, T. (2007) Accumulation of mono-glycosylated form-rich, plaque-forming PrP^{Sc} in the second atypical bovine encephalopathy case in Japan. *Jpn. J. Infect. Dis.* **60**, 305–308
24. Capobianco, R., Casalone, C., Suardi, S., Mangieri, M., Miccolo, C., Limido, L., Catania, M., Rossi, G., Di Fede, G., Giaccone, G., Bruzzone, M.G., Minati, L., Corona, C., Acutis, P., Gelmetti, D., Lombardi, G., Groschup, M.H., Buschmann, A., Zanusso, G., Monaco, S., Caramelli, M., and Tagliavini, F. (2007) Conversion of the BASE prion strain into the BSE strain: The origin of BSE. *PLoS Pathog.* **3**, e31
25. Masujin, K., Shu, Y., Yamakawa, Y., Hagiwara, K., Sata, T., Matsuura, Y., Iwamaru, Y., Imamura, M., Okada, H., Mohri, S., and Yokoyama, T. (2008) Biological and biochemical characterization of L-type-like bovine spongiform encephalopathy (BSE) detected in Japanese black beef cattle. *Prion* **2**, 123–128
26. Comoy, E.E., Casalone, C., Lescoutra-Etchegaray, N., Zanusso, G., Freire, S., Marcé, D., Auvré, F., Ruchoux, M.M., Ferrari, S., Monaco, S., Salès, N., Caramelli, M., Leboulch, P., Brown, P., Lasmézas, C.I., and Deslys, J.P. (2008) Atypical BSE (BASE) transmitted from asymptomatic aging cattle to a primate. *PloS One* **3**, e3017
27. Ono, F., Tase, N., Kurosawa, A., Hiyaoka, A., Ohyama, A., Tezuka, Y., Wada, N., Sato, Y., Tobiume, M., Hagiwara, K., Yamakawa, Y., Terao, K., and Sata, T. (2011) Atypical L-type bovine spongiform encephalopathy (L-BSE) transmission to *Cynomolgus macaques*, a non-human primate. *Jpn. J. Infect. Dis.* **64**, 81–84
28. Nicot, S. and Baron, T. (2011) Strain-specific barriers against bovine prions in hamsters. *J. Virol.* **85**, 1906–1908
29. Riek, R., Hornemann, S., Wider, G., Billeter, M., Glockshuber, R., and Wüthrich, K. (1996) NMR structure of the mouse prion protein domain PrP (121–231). *Nature* **382**, 180–182
30. Donne, D.G., Viles, J.H., Groth, D., Mehlhorn, I., James, T.L., Cohen, F.E., Prusiner, S.B., Wright, P.E., and Dyson, H.J. (1997) Structure of the recombinant full-length hamster prion protein PrP (29–231): The N terminus is highly flexible. *Proc. Natl. Acad. Sci. U S A.* **94**, 13452–13457
31. Zahn, R., Liu, A., Lührs, T., Riek, R., von Schroetter, C., López García, F., Billeter, M., Calzolai, L., Wider, G., and Wüthrich, K. (2000) NMR solution structure of the human prion protein. *Proc. Natl. Acad. Sci. U S A.* **97**, 145–150
32. López García, F., Zahn, R., Riek, R., and Wüthrich, K. (2000) NMR structure of the bovine prion protein. *Proc. Natl. Acad. Sci. U S A.* **97**, 8334–8339
33. Viles, J.H., Donne, D., Kroon, G., Prusiner, S.B., Cohen, F.E., Dyson, H.J., and Wright, P.E. (2001) Local structural plasticity of prion protein. Analysis of NMR relaxation dynamics. *Biochemstry* **40**, 2743–2753
34. Calzolai, L., Lysek, D.A., Pérez, D.R., Güntert, P., and Wüthrich, K. (2005) Prion protein NMR structures of chickens, turtles, and frogs. *Proc. Natl. Acad. Sci. U S A.* **102**, 651–655
35. Gossert, A.D., Bonjour, S., Lysek, D.A., Fiorito, F., and Wüthrich, K. (2005) Prion protein NMR structures of elk and of mouse/elk hybrids. *Proc. Natl. Acad. Sci. U S A.* **102**, 646–650
36. Pettersen, E.F., Goddard, T.D., Huang, C.C., Couch, G.S., Greenblatt, D.M., Meng, E.C., and Ferrin, T.E. (2004) UCSF Chimera—a visualization system for exploratory research and analysis. *J. Comput. Chem.* **25**, 1605–1612
37. Sigurdson, C.J., Nilsson, K.P.R., Hornemann, S., Manco, G., Fernández-Borges, N., Schwarz, P., Castilla, J., Wüthrich, K., and Aguzzi, A. (2010) A molecular switch controls interspecies prion disease transmission in mice. *J. Clin. Invest.* **120**, 2590–2599
38. Wille, H., Michelitsch, M.D., Guénebaut, V., Supattapone, S., Serban, A., Cohen, F.E., Agard, D.A., and Prusiner, S.B. (2002) Structural studies of

the scrapie prion protein by electron crystallography. *Proc. Natl. Acad. Sci. U S A.* **99**, 3563–3568

39. Govaerts, C., Wille, H., Prusiner, S.B., and Cohen, F.E. (2004) Evidence for assembly of prions with left-handed β-helices into trimers. *Proc. Natl. Acad. Sci. U S A.* **101**, 8342–8347
40. Raetz, C.R.H. and Roderick, S.L (1995) A left-handed parallel β helix in the structure of UDP-*N*-acetylglucosamine acyltransferase. *Science* **270**, 997–1000
41. Stork, M., Giese, A., Kretzschmar, H.A., and Tavan, P. (2005) Molecular dynamics simulations indicate a possible role of parallel β-helices in seeded aggregation of poly-Gln. *Biophys. J.* **88**, 2442–2451
42. Langedijk, J.P.M., Fuentes, G., Boshuizen, R., and Bonvin, A.M.J.J. (2006) Two-rung models of a left-handed β-helix for prions explains species barrier and strain variation in transmissible spongiform encephalopathies. *J. Mol. Biol.* **360**, 907–920
43. Kunes, K.C., Clark, S.C., Cox, D.L., and Singh, R.R.P. (2008) Left handed β helix models for mammalian prion fibrils. *Prion* **2**, 81–90
44. Choi, J.H., May, B.C.H., Govaerts, C., and Cohen, F.E. (2009) Site-directed mutagenesis demonstrates the plasticity of the β helix: implications for the structure of the misfolded prion protein. *Structure* **17**, 1014–1023
45. Hara, H., Okemoto-Nakamura, Y., Shinkai-Ouchi, F., Hanada, K., Yamakawa, Y., and Hagiwara, K. (2012) Mouse prion protein (PrP) segment 100 to 104 regulates conversion of PrP^{C} to PrP^{Sc} in prion-infected neuroblastoma cells. *J. Virol.* **86**, 5626–5636
46. Bryan, A.W. Jr, Starner-Kreinbrink, J.L., Hosur, R., Clark, P.L., and Berger, B. (2011) Structure-based prediction reveals capping motifs that inhibit β-helix aggregation. *Proc. Natl. Acad. Sci. U S A.* **108**, 11099–11104
47. DeMarco, M.L. and Daggett, V. (2004) From conversion to aggregation: protofibril formation of the prion protein. *Proc. Natl. Acad. Sci. U S A.* **101**, 2293–2298
48. DeMarco, M.L., Silveira, J., Caughey, B., and Daggett, V. (2006) Structural properties of prion protein protofibrils and fibrils: an experimental assessment of atomic models. *Biochemistry* **45**, 15573–15582
49. Scouras, A.D. and Daggett, V. (2012) Disruption of the X-loop turn of the prion protein linked to scrapie resistance. *Protein Eng. Des. Sel.* **25**, 243–249
50. Priola, S.A. and Chesebro, B. (1995) A single hamster PrP amino acid blocks conversion to protease-resistant PrP in scrapie-infected mouse neuroblastoma cells. *J. Virol.* **69**, 7754–7758
51. Apostol, M.I., Wiltzius, J.J.W., Sawaya, M.R., Cascio, D., and Eisenberg, D. (2011) Atomic structures suggest determinants of transmission barriers in mammalian prion disease. *Biochemistry* **50**, 2456–2463
52. Samson, A.O. and Levitt, M. (2011) Normal modes of prion proteins: From native to infectious particle. *Biochemistry* **50**, 2243–2448
53. Wille, H., Bian, W., McDonald, M., Kendall, A., Colby, D.W., Bloch, L., Ollesch, J., Borovinskiy, A.L., Cohen, F.E., Prusiner, S.B., and Stubbs, G. (2009) Natural and synthetic prion structure from X-ray fiber diffraction. *Proc. Natl. Acad. Sci. U S A.* **106**, 16990–16995
54. Weissmann, C. (2012) Mutation and selection of prions. *PLoS Pathog.* **8**, e1002582

Seminar
セミナー

BSE問題におけるリスク管理とその変遷

中村優子
Yuko OKEMOTO-NAKAMURA
国立感染症研究所細胞化学部
主任研究官

萩原健一
Ken'ichi HAGIWARA
国立感染症研究所細胞化学部
第一室室長

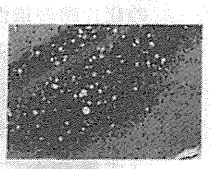

1 はじめに

プリオン病は治療法が確立されていない，難治性・致死性の神経変性疾患である．ウシのプリオン病であるウシ海綿状脳症(bovine spongiform encephalopathy；BSE)とヒトのプリオン病である変異型クロイツフェルト・ヤコブ病(variant Creutzfeldt-Jakob disease；vCJD)との関連性が指摘されてから四半世紀が，また我が国においてBSEの発生が確認されてから10年あまりが経過した．BSE発生国ではBSEやvCJDのリスク管理として様々な対策がとられており，その実効性が徐々に明らかになってきている．本稿では食の安全に関する対策を中心にその概要，そして今日までのBSE・vCJDの発生状況の推移について紹介する．また，BSEに関する新たな知見についても述べる．

2 動物由来感染症としてのプリオン病

プリオン病は，伝達性海綿状脳症(transmissible spongiform encephalopathy；TSE)と呼ばれる疾病の別名である．“海綿状脳症”という言葉に表されるとおり，その病理所見は神経細胞の脱落に伴う脳組織などの空胞変性を特徴とする(右上写真参照)．これまでにヒトを含め，ヒツジ，ウシ，シカなどのTSEが報告されているが(表1)，中でもヒツジのスクレイピーは18世紀に欧州で流行し，古くからその存在が知られていた．スクレイピーはヒツジ個体間での水平感染が起こるが，スクレイピーの発生・流行とヒトのTSEであるクロイツフェルト・ヤコブ病(Creutzfeldt-Jakob disease；CJD)の発生率との間に疫学的な関連性が見られないことから，ヒトはスクレイピー病原体には感染しないと考えられている．

一方，1986年にウシのTSE例が英国において初めて報告され，[1] BSEと名付けられた．BSEが発生したのはスクレイピー病原体に汚染された飼料(肉骨粉)をウシに与えたためであるという説が唱えられているが，確定には至っていない．そしてBSEの発生の増加を追うように，ヒトのvCJDが新たに発生した．

表1 伝達性海綿状脳症(TSE)

自然宿主動物	名称
ヒツジ・ヤギ	スクレイピー
ウシ	ウシ海綿状脳症(BSE)
シカ	慢性消耗病(CWD)
ミンク	伝達性ミンク海綿状脳症
ヒト	クロイツフェルト・ヤコブ病(CJD)
	孤発性(sCJD)；発症原因不明(プリオンタンパク質の自発的な異常化？)
	家族性(fCJD)；プリオンタンパク質遺伝子の変異
	医原性(iCJD)；TSEに汚染された医療器材や生物製剤等の使用
	変異型(vCJD)；BSEに汚染された食品の摂取等
	致死性家族性不眠症(FFI)
	ゲルストマン・ストロイスラー・シャインカー病(GSS)
	クールー

TSEの病原体プリオンは，異常型プリオンタンパク質(PrP^{Sc})からなるタンパク質性の感染因子であり，紫外線照射や通常の高圧処理滅菌，あるいはホルマリン処理では不活化できない．さらに，TSEの有効な治療法は今日でも確立されていない．vCJD患者の発生数は，他の疾患の流行に比べ大規模といえるものではない．しかし，患者数の多少に関わらず致死的な疾患であること，また畜産物を介して不特定多数のヒトがBSEプリオンに曝露される可能性があることから，その対策は緊急の課題となった．中でも食肉などの畜産物へのBSEプリオンの混入を防ぐことは最も重要かつ有効な対策であり，各国で，①新たなBSEの発生を阻止するため

の対策，②BSEに汚染された，あるいは汚染される可能性がある部位の食肉・加工品の流通を禁じる対策，の2つが講じられている．

3 英国におけるBSE・vCJD発生の推移にみる対策の有効性

世界で最初にBSEが報告された英国は，世界最多のBSE発生国でもある．また，vCJDも英国で最初に報告され，患者数は最も多い．以下に，英国のBSE諸対策と，同国でのBSEおよびvCJD発生の推移を振り返って考えてみたい．

英国におけるBSE発生件数は今日までに18万頭にも上る(図1)．BSEの大規模な流行は，ウシに与えられた肉骨粉飼料がBSEプリオンに汚染されており，容易に水平伝播が生じたためと考えられた．そこで講じられた対策が，家畜の飼料規制である．1988年には反すう動物由来のタンパク質を反すう動物へ与えることが禁止され，さらに徹底を図るために，1996年には哺乳動物の肉骨粉飼料の使用および保有が禁止された．BSEは約3～8年の潜伏期間を経て発症するとされており，[2] 上記の規制後の1992年まではBSEの発生増加が続くが，その後は劇的に減少し，2012年(2012年6月現在)は1頭にとどまっている(図1)．この疫学的データから，飼料規制がBSE流行の沈静化に非常に有効であったことが伺える．しかし，頭数は少ないながらも飼料規制後に出生したウシでのBSE発生が続いていることに関しては注意が必要である．飼料の交差汚染が生じているためと指摘されているが，今後もその実態を把握していく必要があるだろう．

一方，BSE発生後に英国におけるCJD発生動向に関する調査が行われた結果，1996年に従来のCJDとは異なる特徴を示す(発症年齢が従来に比べ若い，脳波パターンが異なる，など)10例の新奇のCJD患者の存在が報告された．[3] vCJDの発生である．英国海綿状脳症諮問委員会がvCJDの原因がBSEである可能性が高いと発表し，BSEとvCJDとの疫学的な関連が推察されるなか，近交系マウス，あるいはヒト・プリオンタンパク質(PrP)を発現させた遺伝子改変マウスを用いた伝達実験が進められた．その結果，BSEとvCJD接種群で潜伏期

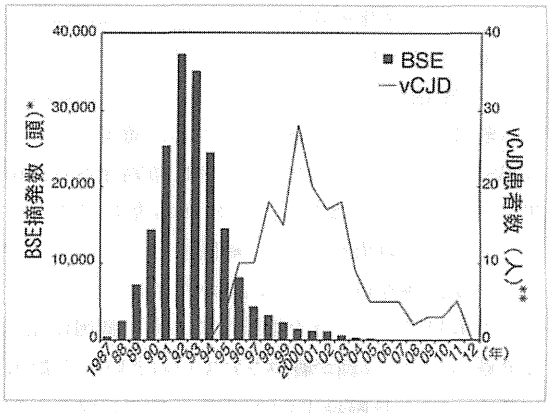

図1 英国におけるBSEおよびvCJD発生状況

* World Organisation for Animal Healthホームページより改変．
** European Creutzfeldt Jakob Disease Surveillance Networkホームページより改変．

間や病変部位の分布が類似していることが1997年に報告され，[4～6] 動物実験においてもBSEとvCJDの因果関係が示唆された．既に1989年よりBSEプリオンが蓄積しやすい特定臓器(脳，脊髄など)の食用への使用が禁止されていたが，その後禁止措置は強化され，2000年をピークにvCJD発生数は減少傾向にある．BSEがvCJDの原因であることを直接的に示す科学的証拠は今日でもないが，上述の疫学的相関やマウスへの感染実験からBSEとvCJDの関連性はほぼ疑いがない．このように，英国で講じられたBSE対策はvCJDのリスク低減に対しても効果的であったように見受けられる．ただし，ヒトのBSEプリオンに対する感受性やvCJDの潜伏期間の長短はPrPの遺伝子多型により異なる可能性が指摘されており，今後も長期間にわたり追跡調査していくことが肝要であろう．

4 日本におけるBSEの発生と対策

日本では2001年9月に国内初のBSEが確認されたのを受け，翌10月には飼料原料として肉骨粉を利用することが全面的に禁止され，また国内のウシ由来の肉骨粉は焼却処分された．さらに，と畜場においてすべてのウシの特定危険部位(舌および頬肉を除く頭部，脊髄および回腸，背根神経節を含む脊柱)の除去が義務付けられ，全月齢のウシを対象としたELISA法によるスクリーニング検査が導入さ